

PL-TR-96-2154

**SEISMIC ATTENUATION STUDIES IN THE
MIDDLE EAST AND SOUTHERN ASIA**

**Brian J. Mitchell
Lianli Cong
Jiakang Xie**

**St Louis University
Department of Earth & Atmospheric Sciences
3507 Laclede Avenue
St Louis, MO 63103**

19 July 1996

19961104 110

Scientific Report No. 1

Approved for public release; distribution unlimited



**PHILLIPS LABORATORY
Directorate of Geophysics
AIR FORCE MATERIEL COMMAND
HANSCOM AFB, MA 01731-3010**

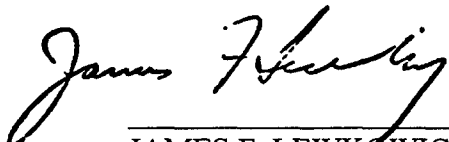
DTIC QUALITY INSPECTED 1

SPONSORED BY
Department of Energy
Office of Non-Proliferation and National Security

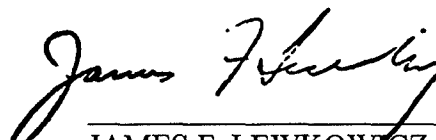
MONITORED BY
Phillips Laboratory
CONTRACT No. F19628-95-K-0004

The views and conclusions contained in this document are those of the authors and should not be interpreted as representing the official policies, either express or implied, of the Air Force or U.S. Government.

This technical report has been reviewed and is approved for publication.



JAMES F. LEWKOWICZ
Contract Manager
Earth Sciences Division



JAMES F. LEWKOWICZ
Director
Earth Sciences Division

This report has been reviewed by the ESD Public Affairs Office (PA) and is releasable to the National Technical Information Service (NTIS).

Qualified requestors may obtain copies from the Defense Technical Information Center. All others should apply to the National Technical Information Service.

If your address has changed, or you wish to be removed from the mailing list, or if the addressee is no longer employed by your organization, please notify PL/IM, 29 Randolph Road, Hanscom AFB, MA 01731-3010. This will assist us in maintaining a current mailing list.

Do not return copies of this report unless contractual obligations or notices on a specific document requires that it be returned.

REPORT DOCUMENTATION PAGE

Form Approved
OMB No. 0704-0188

Public reporting burden for this collection of information is estimated to average 1 hour per response, including the time for reviewing instructions, searching existing data sources, gathering and maintaining the data needed, and completing and reviewing the collection of information. Send comments regarding this burden estimate or any other aspect of this collection of information, including suggestions for reducing this burden, to Washington Headquarters Services, Directorate for Information Operations and Reports, 1215 Jefferson Davis Highway, Suite 1204, Arlington, VA 22202-4302, and to the Office of Management and Budget, Paperwork Reduction Project (0704-0188), Washington, DC 20503.

1. AGENCY USE ONLY (Leave blank)		2. REPORT DATE 19 July 1996		3. REPORT TYPE AND DATES COVERED Scientific No. 1	
4. TITLE AND SUBTITLE Seismic Attenuation Studies in the Middle East and Southern Asia				5. FUNDING NUMBERS PE69120H PRDENN TAGM WUAE Contract F19628-95-K-0004	
6. AUTHOR(S) Brian J. Mitchell Lianli Cong Jiakang Xie					
7. PERFORMING ORGANIZATION NAME(S) AND ADDRESS(ES) Department of Earth & Atmospheric Sciences Saint Louis University 3507 Laclede Avenue St. Louis, MO 63103				8. PERFORMING ORGANIZATION REPORT NUMBER	
9. SPONSORING/MONITORING AGENCY NAME(S) AND ADDRESS(ES) Phillips Laboratory 29 Randolph Road Hanscom AFB, MA 01731-3010 Contract Manager: James F. Lewkowicz/GPE				10. SPONSORING/MONITORING AGENCY REPORT NUMBER PL-TR-96-2154	
11. SUPPLEMENTARY NOTES					
12a. DISTRIBUTION/AVAILABILITY STATEMENT Approved for public release; distribution unlimited				12b. DISTRIBUTION CODE	
13. ABSTRACT (Maximum 200 words) Previous research has indicated that the Middle East and southern Asia are characterized by high attenuation that may be caused by high intrinsic absorption, scattering by complex velocity structure, or both. We are trying to model these attenuative properties by measuring the attenuation of Lg coda waves as well as fundamental-mode surface waves in that region. Determinations of Lg coda Q there have allowed us to complete our map of Lg coda Q for all of Eurasia. Initial determinations of fundamental-mode Rayleigh and Love wave attenuation, using a two-station method indicate that attenuation for those waves, especially at short periods, is very high. This suggests that Q in the upper crust is very low, a result that is consistent with our Lg coda Q results. A new code has been developed for measuring dispersion and polarization properties of surface waves. Initial tests with code indicate that surface wave propagation in the Middle East is often complex and marked by lateral refraction and mode conversion along the paths of propagation.					
14. SUBJECT TERMS Attenuation Q Lg Lg coda Crustal structure Surface waves				15. NUMBER OF PAGES 52	
				16. PRICE CODE	
17. SECURITY CLASSIFICATION OF REPORT Unclassified	18. SECURITY CLASSIFICATION OF THIS PAGE Unclassified	19. SECURITY CLASSIFICATION OF ABSTRACT Unclassified	20. LIMITATION OF ABSTRACT SAR		

Table of Contents

1. The variation of Lg coda Q across Eurasia and its relation to continental evolution	1
Introduction	2
Tectonic Setting and Evolution of Eurasia	3
Data Coverage	6
Data Processing	11
Mapping Lg Coda Q Variations - Method	12
Mapping Lg Coda Q Variations - Results	16
Q_0 and Tectonics	23
Conclusions	24
References	24
2. Surface wave propagation and attenuation in the Middle East	28
Introduction	30
Interstation Determinations of Phase Velocity, Group Velocity, and Attenuation	30
A New Tool for Surface Wave Dispersion and Polarization Analysis	37
References	43

Figure Captions

1. Simplified tectonic map of Eurasia. Shield locations are taken from Burke and Sengör (1986) and the Tethysides complex is simplified from Sengör (1984). 5
2. Map of events used in this study. 7
3. Map of stations that provided data for this study. 8
4. Comparison of seismograms recorded for paths through high-Q (top) and low-Q (bottom) regions. The upper seismogram is from a magnitude 4.5 earthquake in the Norwegian Sea (69.418N, 14.201E) at a distance of 1144 km from station KONO and the lower seismogram is from a magnitude 4.2 earthquake in Sichuan Province, China (29.996N, 99.338E) at a distance of 644 km from station KMI. 9
5. Comparison of SSR plots obtained from the seismograms in Figure 4. Note that the value obtained for frequency dependence (determined from the slope of the least-squares fit line) will depend somewhat on the selected frequency range. 13
6. Sampling patterns for Lg coda used in this study. Each Lg coda is assumed to sample an elliptical area corresponding to the maximum lapse time used in the analysis. When a continental boundary is encountered we assume it is a barrier to Lg propagation and therefore forms part of the boundary for the sampling area. 15
7. Tomographic map of Lg coda Q at 1 Hz for most of Eurasia. 18
8. Tomographic map of the frequency dependence, η , of Lg coda Q at 1 Hz for most of Eurasia. 19
9. Point spreading function (psf) plots for grids centered at 70.93°N - 41.96°E, at 63.79°E - 125.53°E, at 48.77°N - 27.85°E, and at 32.40°N - 96.83°E. 20
10. Error distribution for the Q_0 image of Eurasia. The error is tested empirically, based upon the sample standard error in the Q_0 and η values calculated from real data and the pseudo-random sign generators. See text for details. 21
11. Error distribution for the η image of Eurasia. The error is tested empirically as described in the caption for Figure 10. 22

**The Variation of Lg Coda Q across Eurasia
and its Relation to Continental Evolution**

by

Brian J. Mitchell

Yu Pan

and

Jiakang Xie

Department of Earth and Atmospheric Sciences

Saint Louis University

St. Louis, MO 63103

Introduction

Lg is often the most prominent and robust phase on short-period and broad-band seismograms recorded in continental regions. For that reason it has been used to determine magnitudes of small events at regional distances (Baker, 1970; Nuttli, 1973), yields of nuclear explosions (Nuttli, 1986), and regional variations of crustal attenuative properties (Campillo & Plantee, 1991; Mitchell, 1981; Sutton, Mitronovas, & Pomeroy, 1967). It can be treated as a superposition of higher-mode Rayleigh waves that propagate in the continent crust (Kennett, 1984; Knopoff, Schwab, & Kausel, 1973; Panza & Calcagnile, 1975). The onset of Lg arrives with a group velocity of 3.3 - 3.6 km/s, with young active regions being slower than stable shields.

A coda of up to several minutes duration follows Lg, the predominant frequency of which is lower than the direct phase, and decreases with time. The arrival of Lg coda energy is omnidirectional, indicating that it is scattered from heterogeneities in the crust (Der, Marshall, O'Donnell, & McElfresh, 1984). Being a scattered wave, it is sensitive to properties in a volume of the crust that surrounds the great circle path, including both the seismic source and the receiver, rather than to properties along a single ray path between them. Scattering had earlier been inferred as the cause for coda following body waves at short distances (Aki, 1969; Aki & Chouet, 1975).

The attenuation of both Lg and Lg coda is often expressed as the inverse of a quality factor, Q . In the present paper, we use Q_{Lg} and Q_{Lg}^c to denote, respectively, the quality factors of the direct Lg phase and Lg coda. An advantage that use of Lg coda has over use of the direct Lg phase for studying regional variations of attenuation is that measurements can be made using data from only a single station and do not require knowledge of the source spectrum. Q determinations from direct Lg require either a single-station recording from an event with a known source spectrum (or a spectrum that can be determined) or records from two or more stations that lie on a great-circle path with a seismic event. Q_{Lg}^c determinations are, therefore, usually much more plentiful than those of Q_{Lg} and provide better areal coverage in studies of attenuative properties.

A tomographic method for studying regional variations of Lg coda Q was developed by (Xie & Mitchell, 1990a) and was applied to Africa for frequencies near 1 Hz. It assumes that the area sampled by Lg coda forms an ellipse with the source at one focus and the recording station at the other (Malin, 1978). The areal coverage of the ellipse for a given source-station pair increases with increasing lapse time. Xie and Mitchell (1990a) applied a back-projection inversion technique (Dines & Lytle, 1979) to obtain maps of the variation

of Q_0 and η (Q_{Lg}^c at 1 Hz and its frequency dependence) for all of Africa from many event-station pairs. We present details of the method in later sections.

The African study revealed striking variations in Q_{Lg}^c , with low values characterizing regions in which tectonic activity has occurred since the Mesozoic era. These include the East African rift zone (the most prominent feature on the Q map), the Atlas Mountains, the Cape fold belt, and the Cameroon line. High Q_{Lg}^c values characterize the central portions of the cratons which came together to form Africa about 550 M.y. ago. Mitchell (1995) recently suggested that intermediate values of Q_{Lg}^c that occur in the fold belts between the cratons reflect tectonic activity that occurred during the formation of the African continent in the early Paleozoic era. A revised map of frequency dependence values for Africa (Mitchell, 1995) indicates that η varies inversely with Q_{Lg}^c , with low frequency dependence being characteristic of the cratons and high frequency occurring in the low- Q regions.

This report applies the methods of Xie and Nuttli (Xie & Nuttli, 1988) and (Xie & Mitchell, 1990a) to Eurasia, a composite continent consisting of numerous diverse blocks which began a complex coalescence during the Devonian period, about 370 million years ago (Zonenshain, Kuzmin, & Natapov, 1990). In contrast with Africa, for which the tectonics is dominated by two events (the accretion of the cratons during the Pan-African tectono-thermal event about 550 M.y. ago and the recent extension in the East African rift), Eurasia has undergone numerous and diverse periods of tectonic and organic activity. Moreover, whereas Africa is characterized by relatively low relief and modest sedimentary accumulations, Eurasia contains both the world's highest and lowest points and several of its greatest sedimentary basins. Later sections present maps of Lg coda Q and its frequency dependence at frequencies near 1 Hz for most of Eurasia. We then compare them with results from more localized studies of Q_{Lg} and Q_{Lg}^c as well as with fundamental-mode surface attenuation, and correlate them with tectonic features of Eurasia.

Tectonic Setting and Evolution of Eurasia

Eurasia is a collage of continental blocks that have merged over a long period of time beginning in the early Paleozoic era. The two shields of northern Eurasia, the East European Shield and the Siberian Shield, are believed to have amalgamated from smaller continental blocks and to have become fully formed by about 1700 Ma (Zonenshain, et al., 1990). The East European block collided with North America in the early Paleozoic to form Laurentia, an event recorded by the Caledonian fold belt in Scandinavia, Scotland, and Svalbard. Laurentia and the Siberian block remained separated from one another and from numerous smaller crustal blocks until convergence began in the late Devonian period.

Zonenshain et al. (1990) discuss the formation of Eurasia, with emphasis on the evolution of the crust within the former USSR, while Sengör (1984; 1987) details the evolution of the Tethysides, the orogenic complex that extends from Spain to eastern Asia forming the Alpine-Himalayan-Indonesian mountain ranges. Many major features related to the evolution of Eurasia appear in the simplified tectonic map in Figure 1. Names of tectonic features on that map are mainly taken from Sengör (1984) and Burke (1986) but we replace their terms Serindia and Angara Shield, respectively, with the more widely known terms Tarim Basin and Siberian Shield.

The East European and Siberian shields collided with the Altaid complex and with each other beginning about 310 Ma. Accretion of numerous smaller plates culminated in a single Laurasia about 280 Ma. The Altaids were cemented between the Siberian and East European plates and orogeny occurred at that time forming the Urals at the western margin of the Altaids. At this time convergence also began between the Paleo-Tethys oceanic plate and Laurasia along a 6000 km long zone. As the Paleo-Tethys was consumed beneath the Eurasian margin, parts of the newly formed Neo-Tethys (separated from the Paleo-Tethys by the Cimmerian continent) widened over some of its length.

At 220 Ma the plates were extensively reorganized, with the collision of North China block with Eurasia and the nearly complete closure of Paleo-Tethys. Compression ceased within Eurasia and extension affected parts of western Siberia and the Barents Sea Basin.

The margin of the Africa-Arabia plate began to progressively converge with Eurasia at about 160 Ma gradually closing the Tethys ocean. The breakup of Pangea occurred between 160 and 130 Ma while Africa-Arabia was converging with Laurasia. Eurasia separated from North America at about 80 Ma while, at the same time, exotic terrains from the Pacific continued to be deposited at the eastern margin of the plate.

During the Cenozoic (after 65 Ma) plate convergence began between Eurasia and India in the south, and continued between Eurasia and Africa-Arabia in the southwest, and the Pacific plate in the east. Simultaneously, the width of the Tethys substantially decreased.

The complex evolutionary history of Eurasia has left a geologically diverse continent with much lateral complexity. In addition to features formed at the margins of the colliding plates during the long evolutionary history of Eurasia, some cratonic regions have been covered by younger sediments that may reach great thicknesses. Examples of deep sedimentary basins include those in the Barents shelf (Levshin & Berteussen, 1979) where sediment depths reach about 25 km and the Peri-Caspian basin (Neprochnov, 1968) where they are as thick as 20 km.

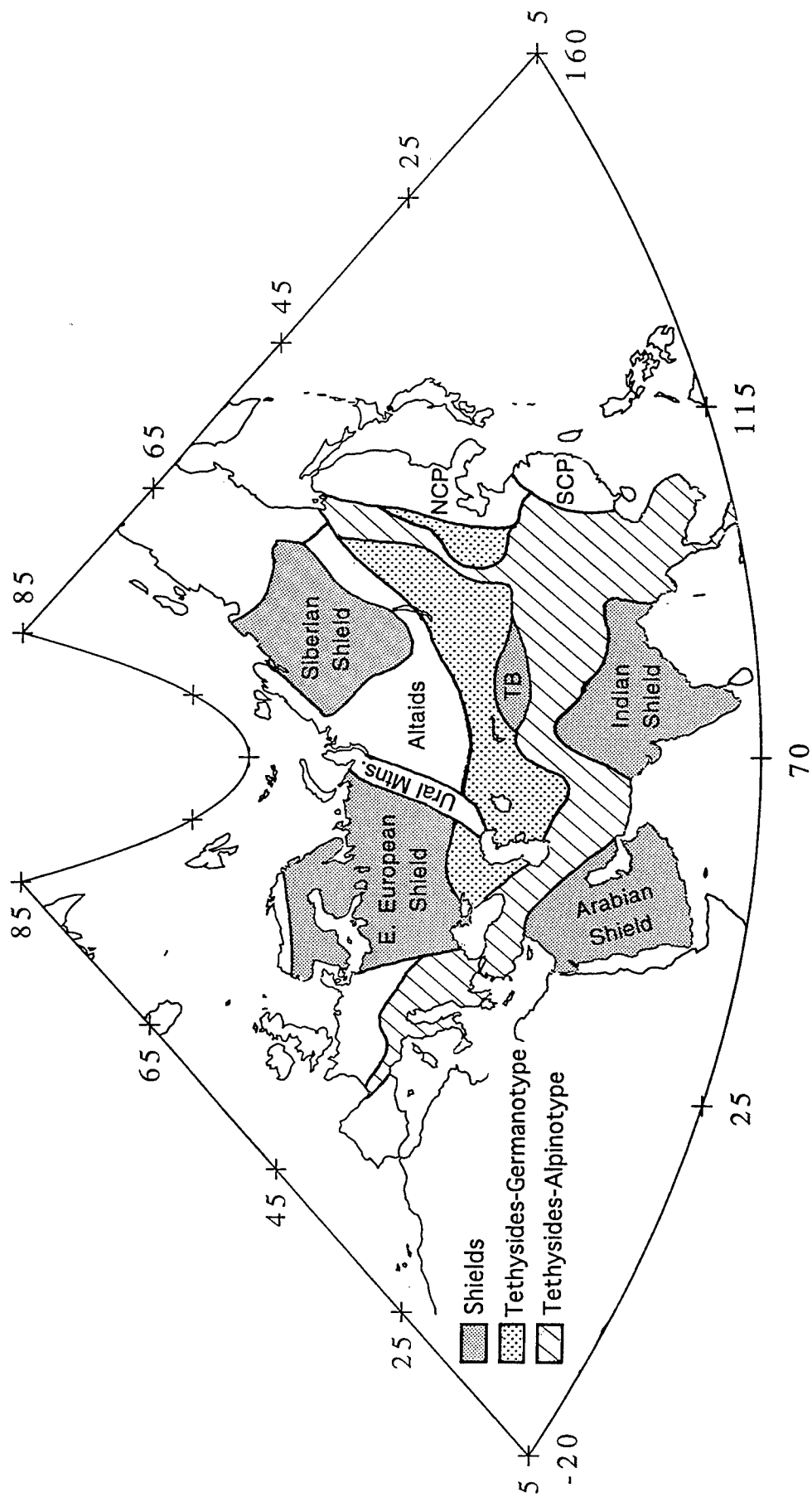


Figure 1

Data Coverage

Data for this study were generated by earthquakes located within or just at the boundaries of the Eurasian plate. We avoided earthquakes outside those boundaries because of the likelihood of systematic errors in Q and its frequency dependence known to be produced when the scattering ellipse associated with any event-station pair includes a significant portion of oceanic crust (Xie & Mitchell, 1990b). Because of the heterogeneity of earthquake occurrence throughout Eurasia, there were many more usable events in the southern portion, especially in China and the Middle East than in the northern portion of the continent (Figure 2).

Recording stations used in this study were widely, and fairly evenly, distributed across Eurasia (Figure 3). Data were obtained from stations belonging to seven different networks of stations (Table 1), some of which provided digital data and some of which provided data in analog form. Digital data were available from networks operated by Incorporated Institutions for Seismology (IRIS), the Chinese Digital Seismic Network (CDSN), the Seismic Research Observatories (SRO), the Digital World-Wide Standard Seismograph Network (DWWSSN), and the Norwegian Seismic Array (NORSAR), while data from stations in the former Soviet Union (MOS), and from the World-Wide Standard Seismograph Network (WWSSN) were in analog form.

All of the Lg coda Q determinations reported in this study are newly determined except those for the Indian subcontinent (John, 1983) and the Arabian peninsula (Ghalib, 1992), which were obtained in earlier studies. We analyzed a few traces in the Arabian Peninsula using the SSR method and found them to be consistent with the earlier obtained values.

This configuration of events and stations in Figures 2 and 3 produced 375 seismograms from 298 seismic events and provided coverage for all of Eurasia except for Spain, Portugal, Italy and Ireland in Europe and for portions of north easternmost and south easternmost Asia and the southern tip of India. The regions in Europe, southeastern Asia, and India lack coverage because it is not possible obtain data there that is not affected by the nearby oceans, whereas the gap in northeastern Siberia occurs because of a lack of station coverage. Data coverage across the rest of Eurasia is, of course, not uniform because of the uneven distribution of events. The best coverage is available for a band that stretches from China to the Middle East because of the large number of events and the relatively good station coverage there.

The character of Lg and its coda varies greatly for different paths in Eurasia. Figure 4 displays two seismograms, one from station KONO in southern Norway produced by an earthquake in the Norwegian Sea and the other from station KMI in southern China

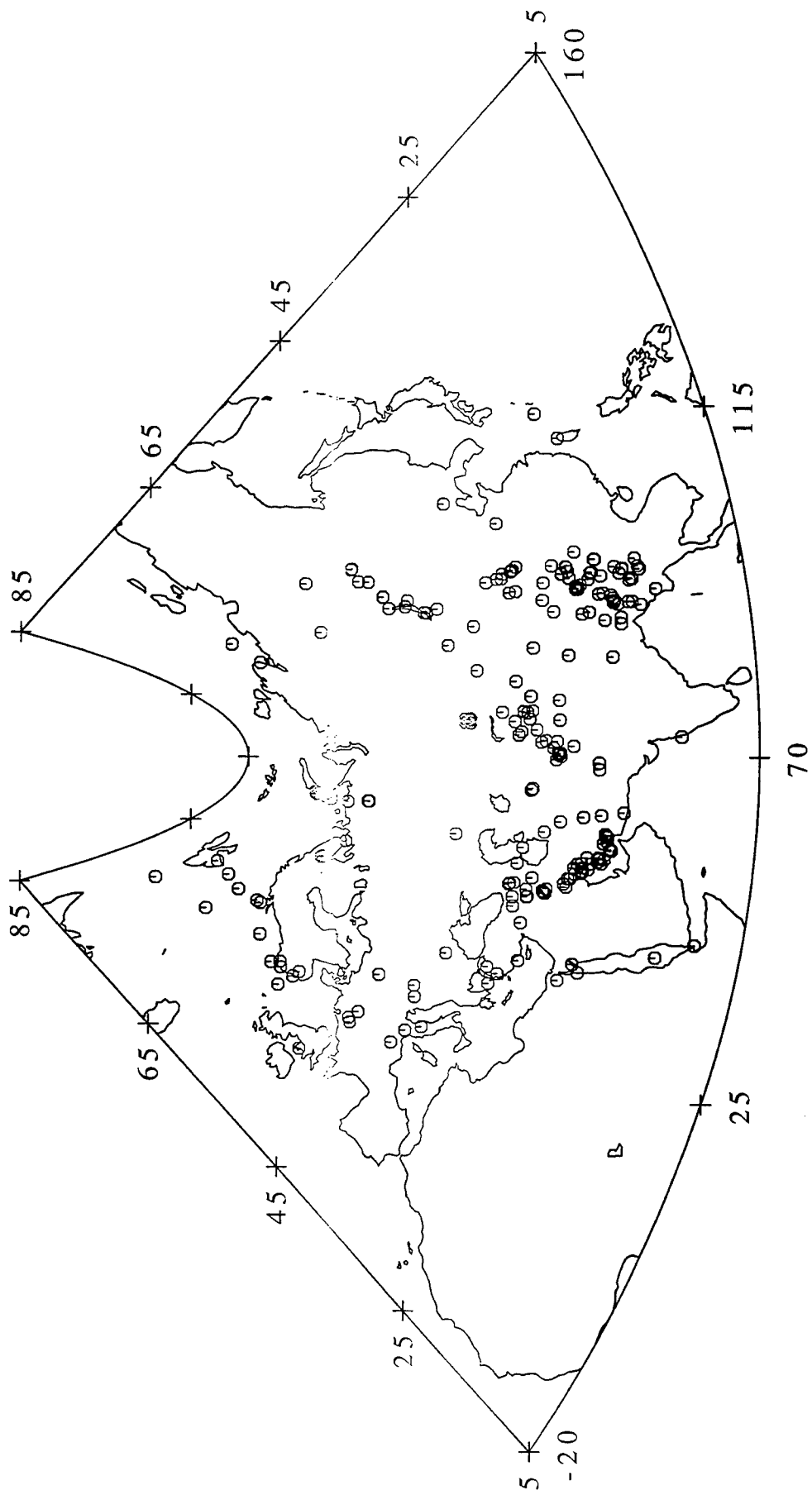


Figure 2

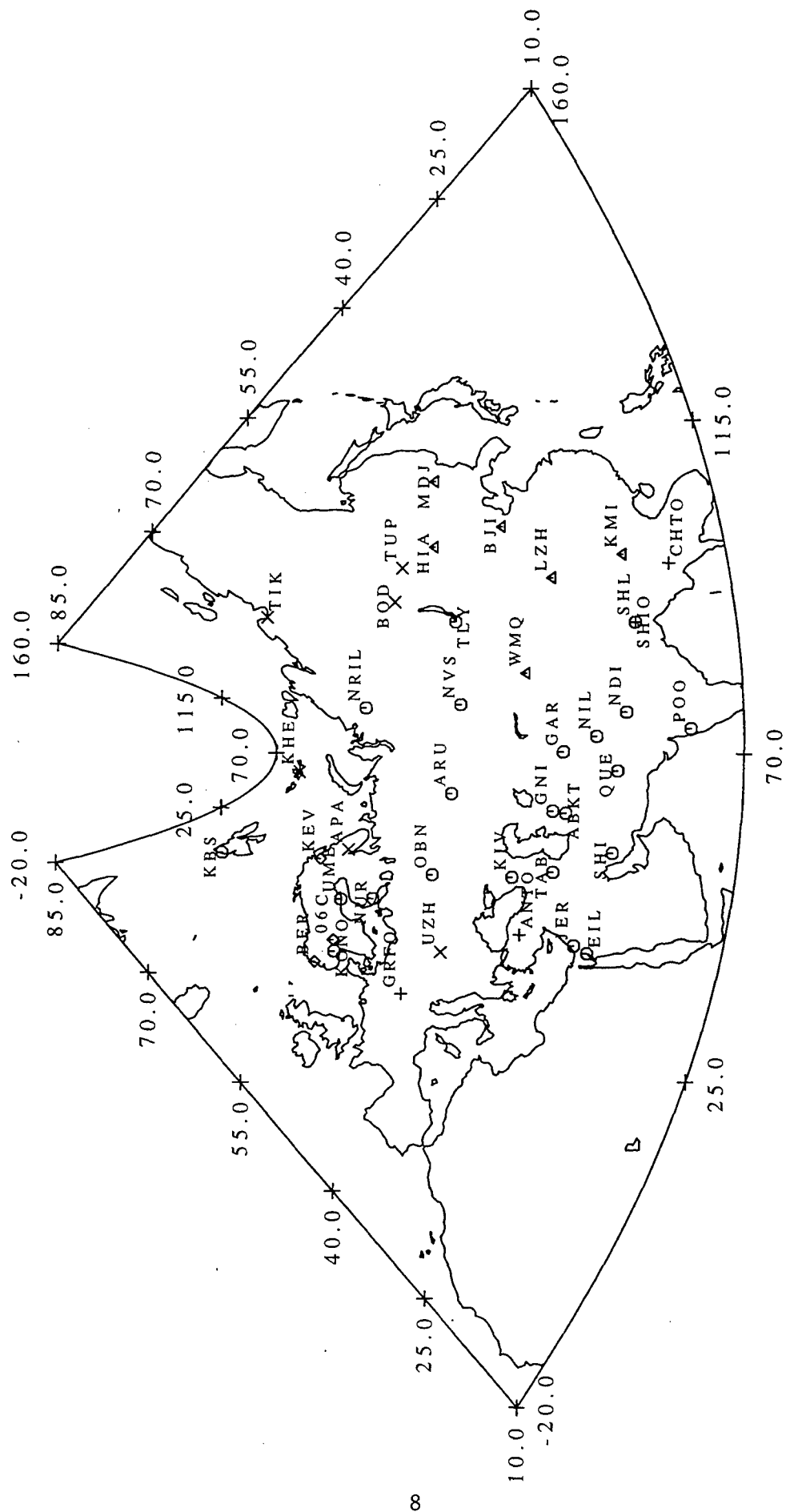


Figure 3

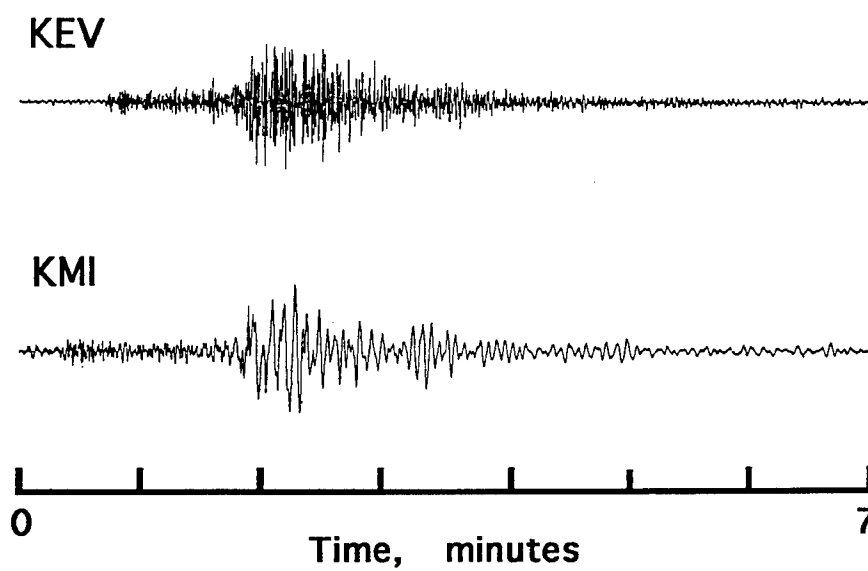


Figure 4

Table 1. Seismographic Stations Used in This Study

Station	Latitude	Longitude	Network
ABKT	37.9304°N	58.1189°E	IRIS
ARU	56.4302°N	58.5625°E	IRIS
GAR	39.0000°N	70.3167°E	IRIS
GNI	40.0530°N	58.1189°E	IRIS
KBS	78.9256°N	11.9417°E	IRIS
KIV	43.9553°N	42.6863°E	IRIS
KONO	59.6491°N	9.5982°E	IRIS
NRIL	69.5049°N	88.4414°E	IRIS
NVS	54.8404°N	83.2346°E	IRIS
OBN	55.1138°N	36.5687°E	IRIS
TLY	51.6807°N	103.6438°E	IRIS
BJI	40.0403°N	116.1750°E	CDSN
HIA	49.2667°N	119.7417°E	CDSN
KMI	25.1233°N	102.7400°E	CDSN
LZH	36.0867°N	103.8444°E	CDSN
MDJ	44.6164°N	129.5919°E	CDSN
WMQ	43.8211°N	87.6950°E	CDSN
ANTO	39.8689°N	32.7936°E	SRO-sp
CHTO	18.8138°N	98.9438°E	SRO-sp
GRFO	49.6919°N	11.2217°E	SRO-sp
SHIO	25.5666°N	91.8830°E	SRO-sp
APA	67.5500°N	33.3333°E	MOS
BOD	57.8499°N	114.1833°E	MOS
KHE	80.6167°N	58.0500°E	MOS
TIK	71.6333°N	128.8667°E	MOS
TUP	54.4333°N	119.9000°E	MOS
UZH	48.6333°N	22.3000°E	MOS
EIL	29.5500°N	34.9500°E	WWSSN-sp
JER	31.7719°N	35.1972°E	WWSSN-sp
NDI	28.6833°N	77.2167°E	WWSSN-sp
NIL	33.6500°N	73.2517°E	WWSSN-sp
NUR	60.5090°N	24.6514°E	WWSSN-sp
POO	18.5333°N	73.8500°E	WWSSN-sp
QUE	30.1883°N	66.9500°E	WWSSN-sp
SHI	29.6445°N	52.5261°E	WWSSN-sp
SHL	25.5667°N	91.8833°E	WWSSN-sp
TAB	38.0675°N	46.3267°E	WWSSN-sp
UME	63.8150°N	20.2367°E	WWSSN-sp
BER	60.3869°N	5.3258°E	DWWSSN-sp
KEV	69.7553°N	27.0067°E	DWWSSN-sp
06C	60.7473°N	11.4583°E	NORSAR

produced by an earthquake in western China. The Lg onset is roughly at 2 minutes from the plot origin in both cases. The predominant frequency is much higher for the KONO record than for the KMI record, even though the event-station distance between the recorded earthquake and KONO is much longer (1144 km) than the event-station distance between the recorded earthquake and KMI (644 km). This obvious depletion of high frequencies at KMI relative to that at KONO indicates that energy is attenuated much more severely in China than it is in Norway. The large difference in frequency content suggests, moreover, that variations in the attenuative properties in different regions of Eurasia can be easily mapped.

The development of Lg coda relative to that of direct Lg for the seismograms of our study is highly variable. Direct Lg is often large and sharp, in which case it is always followed by a coda, but other times it is very emergent, sometimes not easily observed in noise. In that latter case usable Lg coda is often present, but has an emergent beginning and a gradual die-off with time

Data Processing

Xie and Nuttli (1988) developed a stochastic model for the interpretation of single-trace Lg coda waves and an inversion method, based on that model, to determine Lg coda Q and its frequency dependence at 1 Hz (Q_0 and η , respectively). Advantages of their inversion method are that, with data of sufficient quality, tradeoffs between Q_0 and η are avoided (often a problem with earlier methods) and that variances in those quantities are reduced compared to other inversion methods. Application of their stochastic model to examples of recorded ground motion showed that the randomness that occurs in Lg coda waves can be approximated by simple band-limited white Gaussian noise, a result that allows us to make quantitative estimates of variances when estimating Lg coda attenuation.

The inversion method, termed the stacked spectral ratio (SSR) method, has been discussed elsewhere (Xie & Mitchell, 1990a; Xie & Nuttli, 1988); for that reason it is only summarized here. It begins by dividing the Lg coda time series into a number, N_w , of non-overlapping time windows of constant length and applying the discrete Fourier transform to each window to obtain the geometrical mean of the amplitude spectrum at each frequency. The length of each group velocity window for Lg is given by

$$U_m = v\tau_m(1/v_{\min} - 1/v_{\max}) \quad (1)$$

where τ_m is the mean lag time for the m th window, and v , v_{\max} , and v_{\min} are, respectively, the average, maximum, and minimum group velocities of the coda wave train. Geometrical spreading is obtained using

$$G_m = (2\pi R)^{-1/2} (v^2 \tau_m^2 / R^2 - 1)^{-1/4} \quad (2)$$

where R is the event-station distance. The SSR is defined as

$$F_k = \frac{1}{M} \sum_{m=1}^M \frac{1}{\pi(\tau_{M+m} - \tau_m)} \log \left[\frac{G_{M+m} \sqrt{U_m} \langle A_{k,m} \rangle}{G_m \sqrt{U_{M+m}} \langle A_{k,m+M} \rangle} \right] \quad (3)$$

where M is $N_W/2$ when N_W is even and $(N_W + 1)/2$ when N_W is odd. All of the quantities on the right-hand side of (3) are calculable from a coda time series.

Assuming that the frequency dependence of Lg coda Q can be expressed by a power law, $Q(f) = Q_0 f^\eta$, where Q_0 and η are, respectively, Q and its frequency dependence at 1 Hz, then

$$\log F_k = (1 - \eta) \log f_k - \log Q_0 + \varepsilon \quad (4)$$

where ε represents a random error. Theoretical and observational calculations (Xie & Nuttli, 1988) have shown that the SSR provides a statistically stable Q estimator, with the standard error in Q_0 usually being an order of magnitude smaller than Q_0 itself.

The SSR method was applied to all traces beginning at a group velocity of 3.15 km/s and continuing on in time to cover a window length of 300 seconds or more, with the average length being about 450 seconds and the maximum duration being 600 seconds. We tried to minimize variations in coda length from path to path in order to avoid possible systematic biases that might be proportional to coda duration. Using different window lengths for the same seismogram we found that Lg coda Q sometimes increased as much as 20% if coda length was doubled. A similar dependence on coda length was noted in an earlier study using shear waves at shorter distances (Pulli, 1984).

Another possible source of bias in our determinations can arise if a large portion of the scattering ellipse overlaps oceanic regions (Xie & Mitchell, 1990b). For that reason, we avoided events that occurred in oceanic regions as well as continental events for which a large fraction of the scattering ellipse overlaps an oceanic region.

Figure 5 shows example SSR plots for the seismograms in Figure 4. The plots indicate that for station KONO Q_0 (Q_{Lg}^c at 1 Hz) is 770 ± 274 and the frequency dependence (from the slope of the least-squares fit) is 0.12 ± 0.20 , whereas for station KMI Q_0 is 234 ± 66 and frequency dependence is 0.17 ± 0.01 . The plots indicate that if SSR values are linear with frequency over a significant range around the frequency of interest, then reliable values of both Q_0 and η can be obtained.

Mapping Lg Coda Q Variations - Method

Although seismic tomography has been very successful in mapping velocities in the Earth, it has not been used extensively to map variations of attenuative properties. The first such study for regional phases was done for the African continent where a set of Lg coda records that covered much of the continent was assembled and the SSR method was

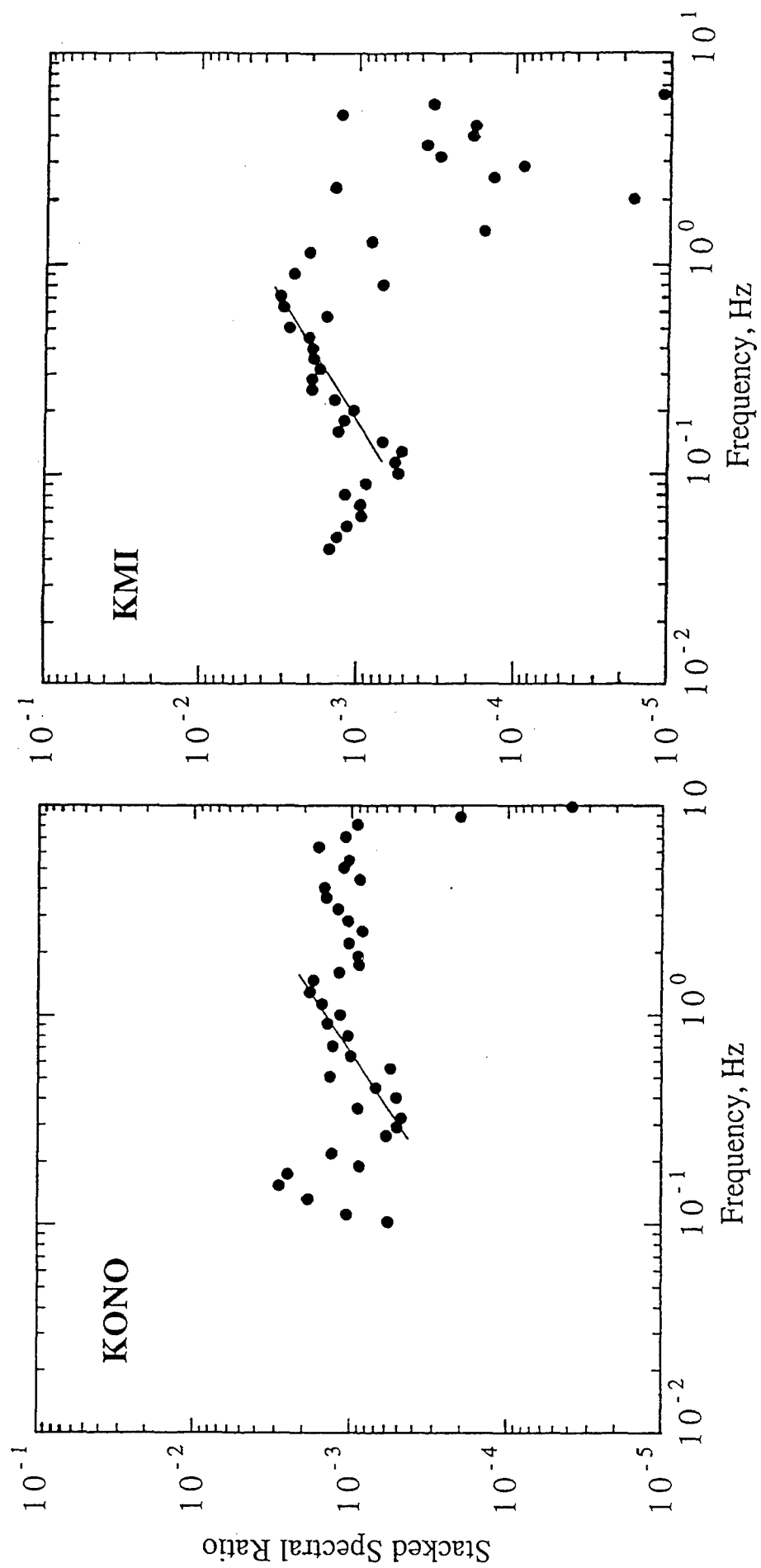


Figure 5

applied to them (Xie & Mitchell, 1990a). The resulting tomographic image revealed striking regional variations of Lg coda Q that coincide with some of the major tectonic features of Africa.

In the present study we apply the same method to Eurasia. It is a back-projection algorithm that produces a tomographic image of Q_{Lg}^c over any broad region using a number (N_c) of individual determinations of Q_{Lg}^c from Lg coda recordings within that region. Since Lg coda consists of scattered waves the energy arriving at a recording station does not follow a straight path between from the seismic event, but is contained within a volume of the crust that includes the source and recording station.

For single scattering the surface projection of the scattered energy takes the form of an ellipse with the source at one focus and the recording station at the other (Malin, 1978). The ellipses cover larger and larger areas as lag time of the coda increases. The elliptical areas for the event-station pairs used in Eurasia are shown in Figure 6 at the maximum lapse time used for the SSR analysis described earlier. If coda waves are scattered through a volume as approximated by the elliptical surface projections in Figure 6, and if many events and recording stations are available, then much overlap occurs among some of the ellipses. This overlap provides data redundancy that is ideal for applying modern inversion techniques to map regional variations of attenuation. The process for doing that is described in the following paragraphs.

To apply the tomographic method we divide the region of interest (in the present case, most of Eurasia) into a number, N_c , of cells that are small enough to allow us to resolve large-scale tectonic features. Q_m , Lg coda Q within the mth cell, is assumed to be constant throughout the cell. For Eurasia, we take the cell dimensions to be $3^\circ \times 3^\circ$. Q_n , the Lg coda Q value calculated for the nth time series, gives the areal average of Lg coda Q over the elliptical area sampled by the coda waves received at the maximum lapse of the Lg coda waves of interest. If we denote the area that the nth ellipse overlaps the mth grid by s_{mn} , then

$$\frac{1}{Q_n} = \frac{1}{S_n} \sum_{m=1}^{N_c} \frac{s_{mn}}{Q_m} + \epsilon_n, \quad n=1, 2, \dots, N_d \quad (5)$$

where

$$S_n = \sum_{j=1}^{N_c} s_{jn} \quad (6)$$

and ϵ_n is the residual due to the errors in the measurement and modeling Lg coda. We solve (5) by a back-projection, or ART technique (Gordon, 1974), that has been used successfully in seismic velocity tomography (Humphreys & Clayton, 1988; McMechan,

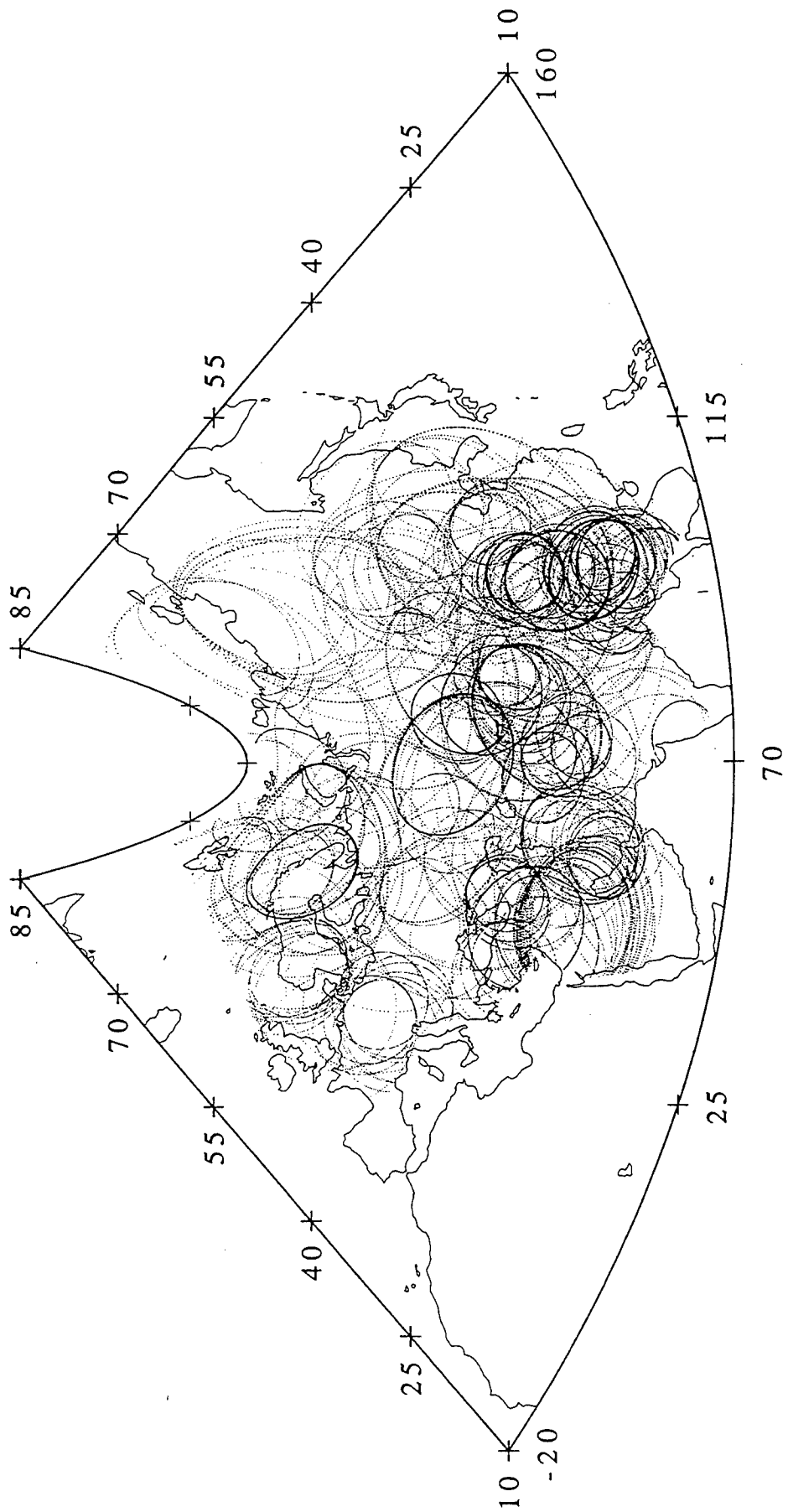


Figure 6

1983; Suetsugu & Nakanishi, 1985). The numerical procedure for that solution is described by Xie and Mitchell (1990a) and will not be repeated here.

A disadvantage of the back-projection technique is that it does not provide formal estimates of resolution or standard error. Humphreys and Clayton (1988) have, however, suggested using a “point spreading function” as an approximation for the resolution kernel. The point spreading function (hereafter abbreviated psf) is obtained by constructing a model in which Q^{-1} has the value of unity in a single cell at the geographical point of interest and is zero everywhere else. We then compute synthetic data using this model and perform an inversion. The resulting image gives the psf at the point of interest, a quantity whose area and falloff with distance gives a measure of resolution.

The effect that random noise in our Lg coda has on our tomographic images can be empirically tested using the sample standard error in Q_n caused by randomness of the SSR's (Xie & Nuttli, 1988). If the standard error for each determination of Q_n is denoted by δQ_n , we can construct a noise series for each Lg coda time series that has an absolute value equal to δQ_n and a sign that is chosen randomly. The n th term of the noise series is added to Q_n and the sum of the two series are then inverted to obtain a new Q_m image. The difference between this image and the original one gives us an error estimate for the Q_m values. Since the sign of δQ_n is chosen by a random binary generator, the process should be repeated several times to obtain an average error estimate.

Mapping Lg Coda Q Variations - Results

We used the back projection method described above to image lateral variations of Lg coda Q across most of Eurasia. The area for which data were available extends between about 15° N and nearly 85° N and between about 10° W and about 160° W. The map depicting Lg coda scattering ellipses (Figure 6) indicates the extent of our data coverage for the Eurasian plate. Northern Eurasia is at high latitudes where the area of any n -degree by n -degree cell covers a much smaller than it does at lower latitudes. In order that the scattering ellipses cover approximately the same number of cells at both and low latitudes, before dividing Eurasia into cells, we performed a coordinate transformation to center Eurasia at the equator. After that transformation, we divided the area of study into 3° by 3° cells and inverted our Q_0 values to obtain a tomographic image of Eurasia. Following the inversion, we transformed the image to its original position. Although this process produces approximately uniform weighting for all cells in Eurasia, it distorts the image at high latitudes.

Lateral variations of Q_0 and η

For our inversion process, using equation 5, we used a starting a starting model in which $Q_m^o = 600$, $m = 1, 2, \dots, N_g$ for the entire region of study. The equation was inverted, after substituting in values for the various areas and determined Q_o values for Q_n . Residuals were calculated for each iteration and the stopping criterion was either that the number of iterations is 20 or the relative change in the sum of squares of residuals is less than 10^{-5} . Figure 7 displays the tomographic image of Q_o for Eurasia. Q_o ranges between about 200 and about 1000, with the high values being centered at three widely separated points.

The process for determining the frequency dependence of Lg coda Q begins by using the Q_o and η values obtained for each trace to estimate Lg coda Q at another frequency; that being 3 Hz in this study. These new values were used as Q_n in equation 5 and a map Lg coda Q at 3 Hz was then obtained. Using the maps of Lg coda Q at 1 Hz and 3 Hz we calculate the frequency dependence of Lg coda Q using the relationship

$$\eta = \frac{1}{\ln 3} \ln \left[\frac{Q(f)_{3Hz}}{Q_o} \right]. \quad (7)$$

Figure 8 shows the distribution of η across Eurasia resulting from this process.

Figures 7 and 8 do not suggest any clear relationship between Q_o and η for Eurasia as has been suggested by (Nuttli, 1988). Possible relationships of those quantities to the tectonics of Eurasia are, however, discussed in the next major section.

Resolution and Error

Figure 9 presents psf plots for four selected regions of Eurasia. As discussed earlier, the areas covered by these plots and the rapidity of their falloff with distance from the center cell can be used to estimate our ability to resolve features of the mapped Q_o and η distributions. Of the four psf plots the best resolution occurs in China where data coverage is densest and the poorest resolution is in northeastern Asia where coverage is the poorest.

The method described in the previous section permits estimates of the effect of random errors in Lg coda Q measurements on our images of Q_o and η . Five tests were run to estimate the error in the images of the two quantities. In each of the tests we constructed two noise series, in both of which the absolute values of the nth terms equal the standard errors found for Q_o and η from the nth coda seismogram. The signs of the nth terms were randomly generated by a random binary generator. The nth terms of the two noise series were then added to the nth measurements of Q_o and η measurements to construct new synthetic maps of Q_o and η . The differences between these new maps and the original ones were calculated and stored after each test. The average values of the differences for the five tests give empirical estimates of absolute error in Q_o and η as shown in Figures 10 and 11.

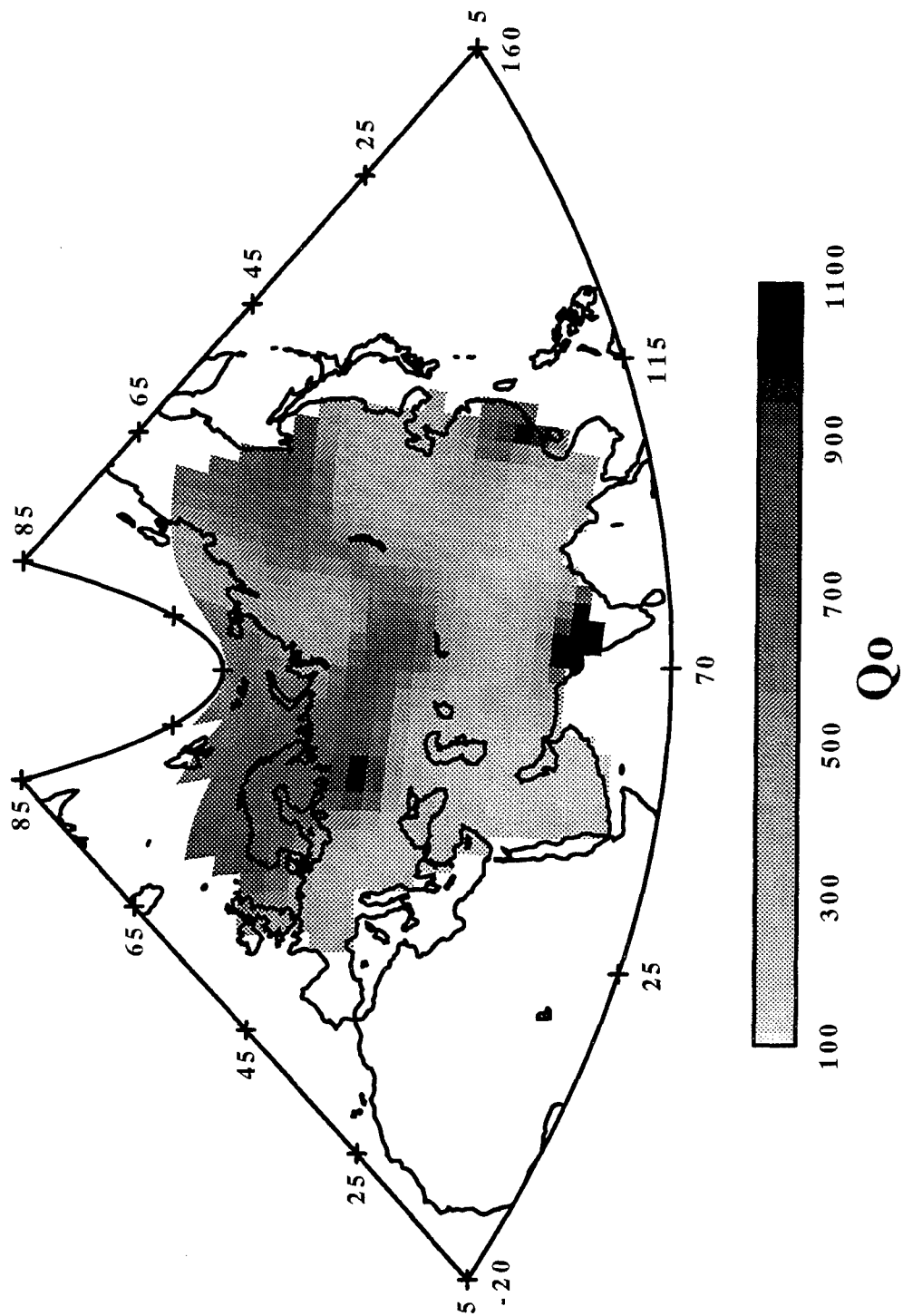


Figure 7

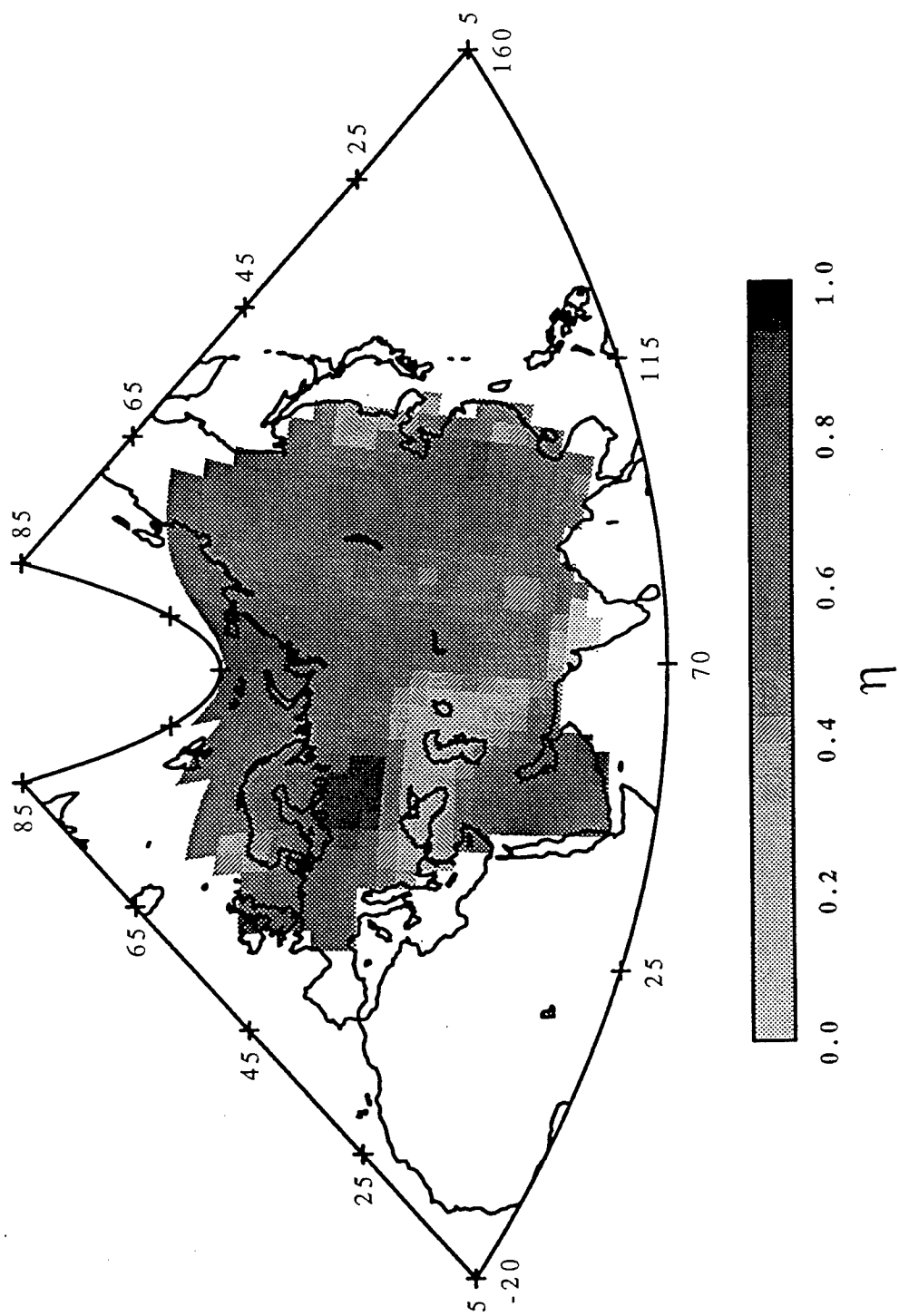


Figure 8

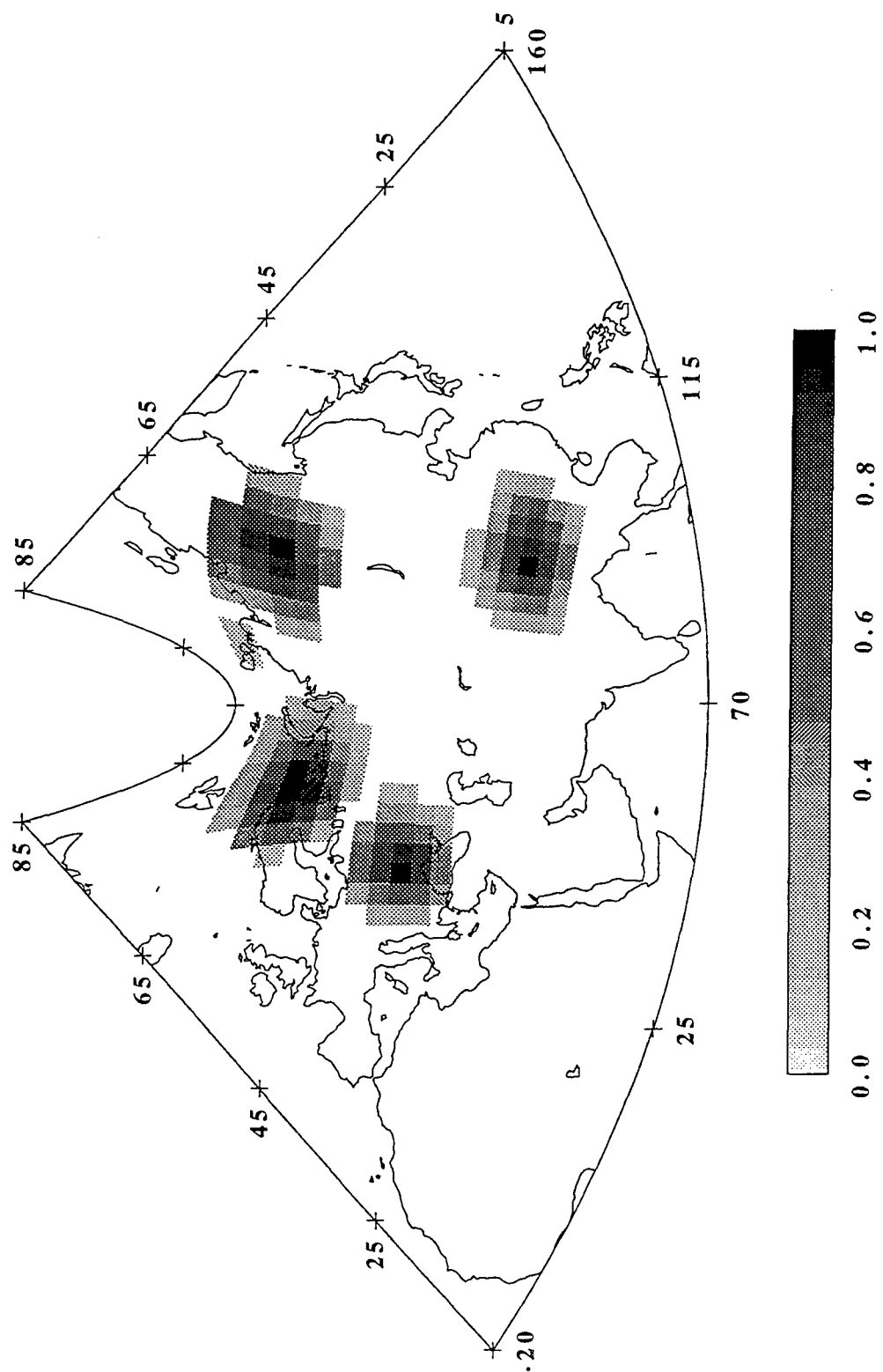


Figure 9

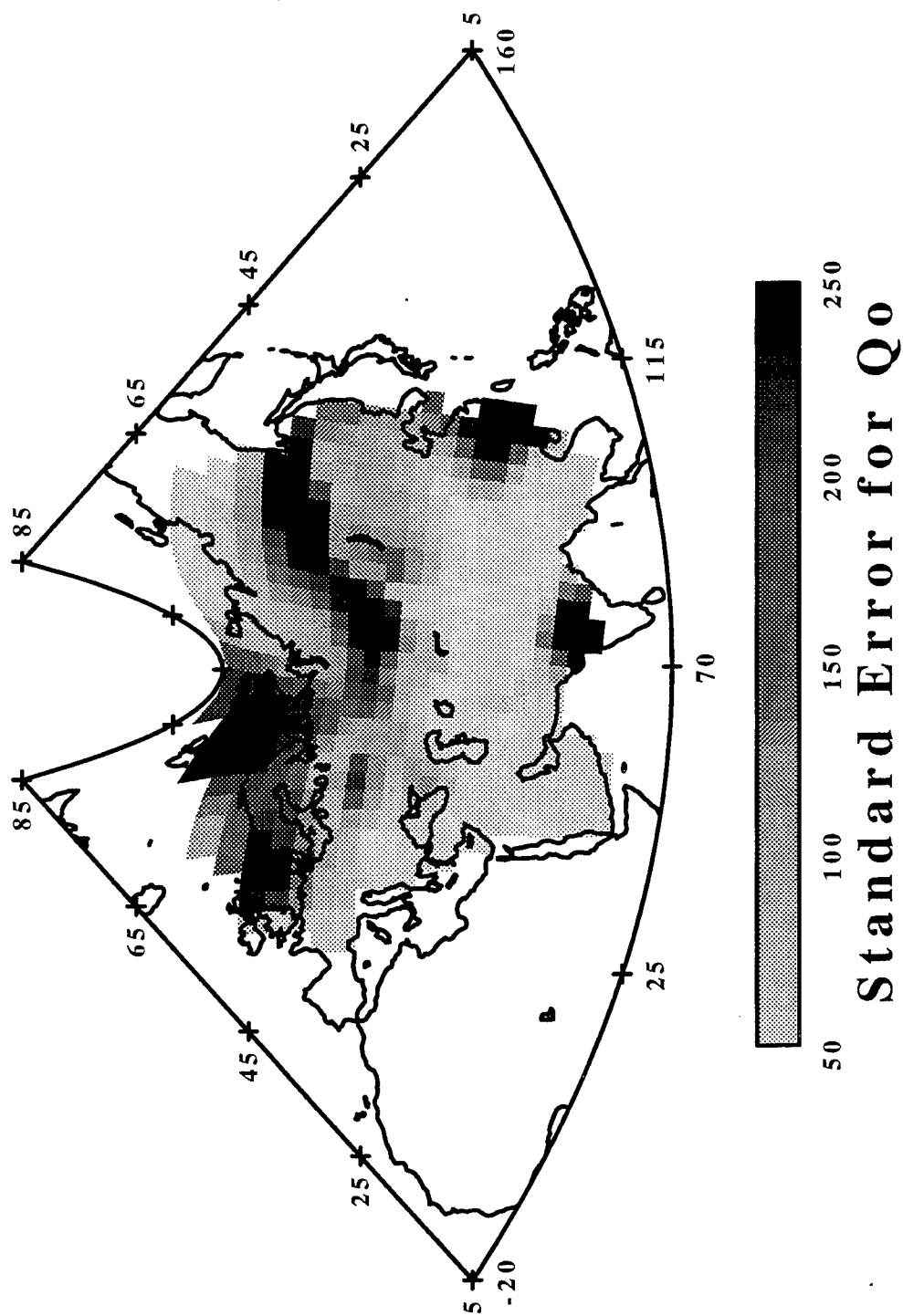


Figure 10

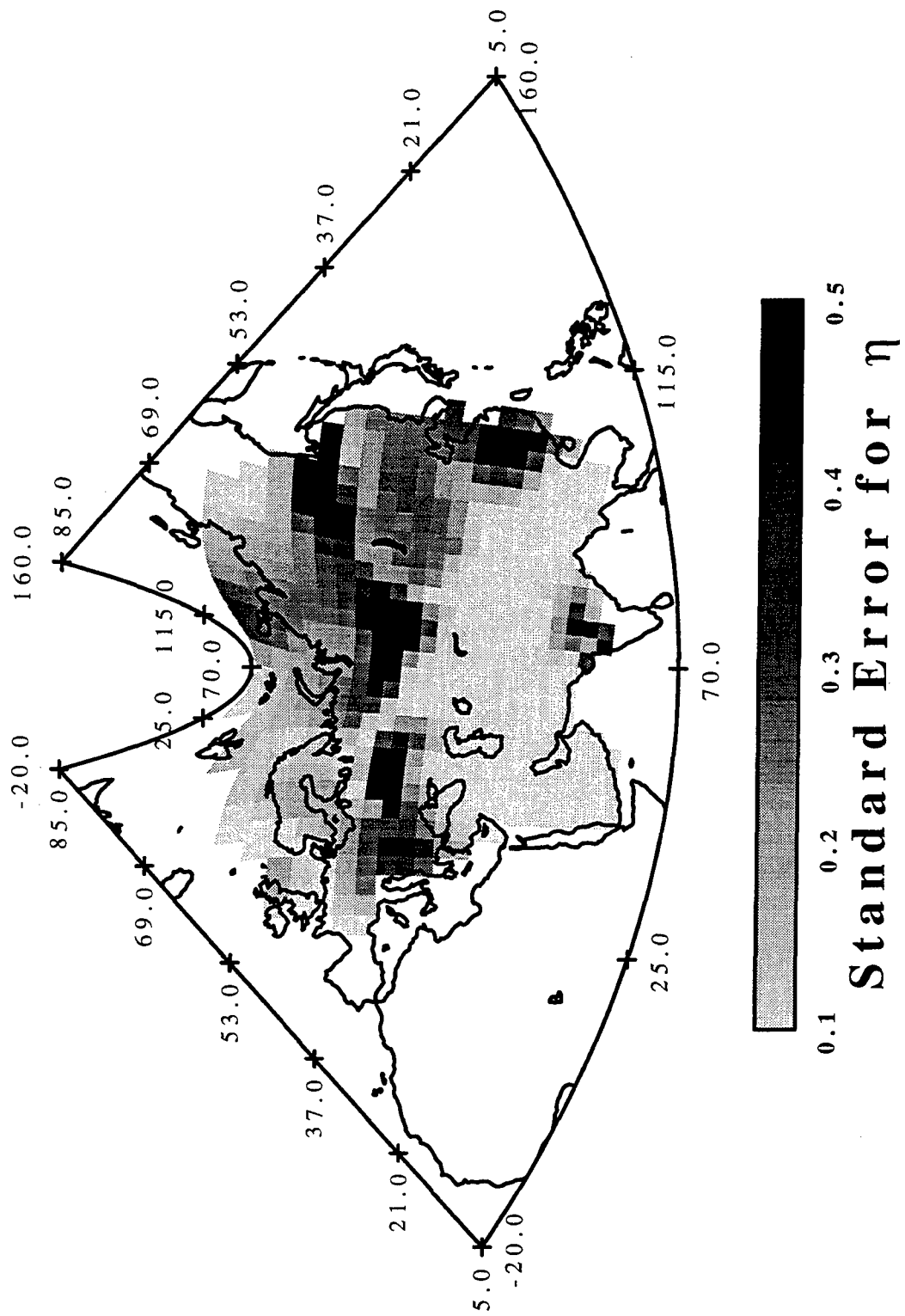


Figure 11

The largest errors in both the Q_0 and η maps largely coincide with the higher Q_0 values in Figure 10. Fractional errors are, however, with some exceptions, relatively uniform throughout Eurasia. It is perhaps noteworthy that the errors are quite high in a region within the East European Shield, where both Q_0 and η are high, a situation that contrasts with the expected relationship between Q_0 and η (Nuttli, 1988).

Comparison of mapped Q_0 with values obtained in regional studies

Several determinations of Lg Q and Lg coda Q have been made in localized studies in Eurasia. In places where both quantities have been determined they commonly take on similar values (Der, et al., 1984; Nuttli, 1988; Xie & Nuttli, 1988). For that reason we have compared Q_0 values determined in the present study with regionally derived values for both Lg Q and Lg coda Q . The Q_0 and η values in eastern China (Figures 7 and 8) are similar to those obtained in a localized study of Lg coda Q there (Chun, Liu, Zhu, & Shih, 1994). Similarly, regional-scale studies of Lg Q in the Barents shelf (Nuttli, 1988), in Iran (Nuttli, 1980), central Asia (Xie, Cong, & Mitchell, 1996), and the Tibetan Plateau (McNamara, Owens, & Walter, 1996) have yielded values that are consistent with those of the continent-scale measurements (Figure 7).

Q_0 and Tectonics

Figure 7 shows three regions where Q_0 is higher than in surrounding regions. One is a broad band that extends from Scandinavia and the Barents shelf through all of northern Asia except for one roughly circular region centered to the southeast of Novaya Zemlya. This band coincides with the two shields of northern Eurasia, the Ural Mountains and the Altaid belt between them. A long broad band with low Q_0 extends from the southern part of western Europe, through the Middle East and central Asia, into China and southeastern Siberia.

Most of the low Q 's in Figure 7 correspond with the Tethysides tectonic region of Figure 1, but they also cover the Arabian Peninsula, a shield region, where high Q 's are normally expected. The Tethysides is a deformed region that began forming about 280 My ago when the Paleo-Tethys Ocean began to be consumed beneath Eurasia. The Alpinotype Tethysides (Figure 1) form the southern portion of the Tethysides and have been deformed as a consequence of orogeny while the Germanotype Tethysides are a more northerly band that consists primarily of dominantly brittle, blocky structures such as grabens, block uplifts, and large strike-slip fault systems (Sengör, 1984).

Another shield where our map exhibits low Q values is the Tarim block in central Asia. The low values there might occur because that small plate is located within the Tethysides complex or because the resolution in our inversion is not sufficient to detect it. High Q

values in the South China Platform are not unexpected since that region has been relatively stable for a long time.

Conclusions

Lg coda Q throughout Eurasia exhibits large regional variations, between about 1000 and 200. The high values are confined to northern Eurasia, in a long, broad band that extends from western Europe through northeastern Siberia, and to the Indian shield and South China Platform. Except for the latter two regions, all of southern Eurasia is characterized by low Lg coda Q, with the lowest values occurring in the southernmost regions. These regions include those that have been most intensely deformed by the Tethysides orogeny and the Arabian Peninsula. The latter region was intensely deformed in its eastern portion while its western portion is being affected by process occurring during the spreading of the Red Sea. Low Q's in the Siberian craton lie in a region that was deformed during the Mesozoic era.

The patterns of Q variation across Eurasia are consistent with the idea that Q in the upper crust is directly proportional to the length of time that has passed since the last major orogeny in any region. In addition, however, the observation that Q's in the Germanotype Tethysides are higher than those in the Alpinotype Tethysides suggest that the intensity of deformation is also important in controlling Q in the upper crust, with Q in more intensely deformed regions being lower than in less deformed regions.

References

- Aki, K. (1969). Analysis of the seismic coda of local earthquakes as scattered waves. Journal of Geophysical Research, 74, 615-631.
- Aki, K., & Chouet, B. (1975). Origin of coda waves: source, attenuation, and scattering effects. Journal of Geophysical Research, 80, 3322-3342.
- Baker, R. G. (1970). Determining magnitude from Lg. Bull. Seism. Soc. Am., 60, 1907-1919.
- Burke, K., & Sengör, C. (1986). Tectonic escape in the evolution of the continental crust. In M. Barazangi (Ed.), Reflection Seismology: The continental crust (pp. 41-53). Washington, DC: Am. Geophys. Union.

- Campillo, M., & Plantee, J. L. (1991). Frequency dependence and spatial distribution of seismic attenuation in France: Experimental results and possible interpretation. Phys. Earth Planet. Int., 67, 48-65.
- Chun, K.-Y., Liu, J., Zhu, T., & Shih, X. R. (1994). Abnormal Lg coda Q in Beijing area. Geophys. Res. Ltr., 21, 317-320.
- Der, Z. A., Marshall, M. E., O'Donnell, A., & McElfresh, T. W. (1984). Spatial coherence structure and attenuation of the Lg phase, site effects, and the interpretation of the Lg coda. Bulletin of the Seismological Society of America, 74, 1125-1147.
- Dines, K. A., & Lytle, R. J. (1979). Computerized geophysical tomography. Proc. IEEE, 67, 1065-1073.
- Ghalib, H. (1992). Seismic velocity structure and attenuation of the Arabian plate. Ph.D. Diss., Saint Louis Univ., 314 pp.
- Gordon, R. (1974). A tutorial on ART. IEEE Trans. Nucl. Sci., NS-21, 78-93.
- Humphreys, E., & Clayton, R. W. (1988). Adaptation of back projection tomography to seismic travel time problems. J. Geophys. Res., 93, 1073-1086.
- John, V. (1983). Coda-Q studies in the Indian subcontinent. M.S. Thesis, Saint Louis University.
- Kennett, B. L. N. (1984). Guided wave propagation in laterally varying media – I. Theoretical development. Geophys. J. Roy. Astr. Soc., 79, 235-255.
- Knopoff, L., Schwab, F., & Kausel, E. (1973). Interpretation of Lg. Geophysical Journal of the Royal Astronomical Society, 33, 389-404.
- Levshin, A., & Berteussen, K. A. (1979). Anomalous propagation of surface waves in the Barents Sea as inferred from NORSAR recordings. Geophys. J. Roy. Astr. Soc., 56, 97-118.

- Malin, P. E. (1978). A first order scattering solution for modeling lunar and terrestrial seismic coda. Ph.D., Princeton Univ.
- McMechan, G. A. (1983). Seismic tomography in boreholes. Geophys. J. Roy. Astr. Soc., 74, 601-612.
- McNamara, D. E., Owens, T. J., & Walter, W. R. (1996). Propagation characteristics of Lg across the Tibetan Plateau. Bull. Seism. Soc. Am., 86, 457-469.
- Mitchell, B. J. (1981). Regional variation and frequency dependence of Q_β in the crust of the United States. Bulletin of the Seismological Society of America, 71, 1531-1538.
- Mitchell, B. J. (1995). Anelastic structure and evolution of the continental crust and upper mantle from seismic surface wave attenuation. Reviews of Geophysics, 33, 441-462.
- Neprochnov, Y. P. (1968). Structure of the earth's crust of epi-continental seas: Caspian, Black, and Mediterranean. Can. J. Earth Sci., 5, 1037-1043.
- Nuttli, O. W. (1973). Seismic wave attenuation and magnitude relations for eastern North America. Journal of Geophysical Research, 78, 876-885.
- Nuttli, O. W. (1980). The excitation and attenuation of seismic crustal phases in Iran. Bulletin of the Seismological Society of America, 70, 469-485.
- Nuttli, O. W. (1986). Yield estimates of Nevada test site explosions obtained from seismic Lg waves. Journal of Geophysical Research, 91, 2137-2152.
- Nuttli, O. W. (1988). Lg magnitudes and yield estimates for underground Novaya Zemlya nuclear explosions. Bulletin of the Seismological Society of America, 78, 873-884.
- Panza, G. F., & Calcagnile, G. (1975). Lg, Li, and Rg from Rayleigh modes. Geophys. J. Roy. Astr. Soc., 40, 475-487.
- Pulli, J. J. (1984). Attenuation of coda waves in New England. Bulletin of the Seismological Society of America, 74, 1149-1166.

Sengör, A. M. C. (1984). The Cimmeride orogenic system and the tectonics of Eurasia. In Geol. Soc. Am. Spec. Pap. No. 195 (pp. 213-244).

Sengör, A. M. C. (1987). Tectonics of the Tethysides: Orogenic collage development in a collisional setting. In G. W. Wetherill, A. L. Albee, & F. G. Stehli (Eds.), Ann. Rev. Earth Sci. (pp. 213-244). Palo Alto, CA: Annual Reviews, Inc.

Suetsugu, D., & Nakanishi, I. (1985). Tomographic inversion and resolution for Rayleigh wave phase velocities in the Pacific Ocean. J. Phys. Earth, 33, 345-368.

Sutton, G. H., Mitronovas, W., & Pomeroy, P. W. (1967). Short-period seismic energy radiation patterns from underground nuclear explosions and small-magnitude earthquakes. Bulletin of the Seismological Society of America, 57, 249-267.

Xie, J., Cong, L., & Mitchell, B. J. (1996). Spectral characteristics of the excitation and propagation of Lg from underground nuclear explosions in central Asia. Journal of Geophysical Research, 101, 5813-5822.

Xie, J., & Mitchell, B. J. (1990a). A back-projection method for imaging large-scale lateral variations of Lg coda Q with application to continental Africa. Geophysical Journal International, 100, 161-181.

Xie, J. K., & Mitchell, B. J. (1990b). Attenuation of multiphase surface waves in the Basin and Range province, Part I: Lg and Lg coda. Geophysical Journal International, 102, 121-137.

Xie, J. K., & Nuttli, O. W. (1988). Interpretation of high-frequency coda at large distances: Stochastic modeling and method of inversion. Geophysical Journal, 95, 579-595.

Zonenshain, L. P., Kuzmin, M. I., & Natapov, L. M. (1990). Geology of the USSR: A Plate-tectonic Synthesis. Washington, DC: Am. Geophys. Union.

Surface-wave Propagation and Attenuation in the Middle East

by

Lianli Cong

Brian J. Mitchell

and

Jiangchuan Ni

Department of Earth and Atmospheric Sciences

Saint Louis University

St. Louis, MO 63103

Figure Captions

- | | |
|--|----|
| 1. Map of events (+) and stations used for inter-station determinations of phase velocity, group velocity, and attenuation in the Middle East. | 31 |
| 2. Single-station surface wave velocity determinations at station GNI for the earthquake of 29 November 1994. | 32 |
| 3. Single-station surface wave velocity determinations at station ANTO for the earthquake of 29 November 1994. | 33 |
| 4. Inter-station surface wave velocity determinations between stations ANTO and GNI for the earthquake of 29 November 1994. | 34 |
| 5. Inter-station phase and group velocities for the station pairs in Figure 1. | 35 |
| 6. Inter-station attenuation coefficients for the station pairs in Figure 1. | 38 |
| 7. Top- Synthetic seismograms for fundamental and higher modes for a crustal model of the eastern United States. The window delineates the time interval over which amplitude spectra were determined. Bottom - Amplitude spectra computed for the traces above. The three traces and spectra correspond to vertical, radial, and transverse components. | 40 |
| 8. Contoured spectral amplitudes obtained after multiple filter analysis of the synthetic seismograms in Figure 7. The largest amplitudes correspond to the expected group velocities of fundamental-mode waves. Smaller, but still easily visible, amplitudes at group velocities near 3.5 km/s correspond to higher-mode surface waves. | 41 |
| 9. Polarization parameters (inclination angle, tilt angle, and slope angle) and ellipticity for the Rayleigh wave ground motion in Figure 7. | 42 |

Introduction

This report describes our work on fundamental-mode surface wave propagation in the Middle East. For that work we are proceeding, simultaneously in two areas: (1) Determination of phase velocities, group velocities, and attenuation coefficients for surface waves in the Middle East, and (2) the development of an interactive GUI code for determining the dispersion and polarization of seismic waves. Progress in each of these areas is described in the following paragraphs.

Interstation Determinations of phase velocity, group velocity, and attenuation

We searched for earthquakes near great-circle paths that pass between various pairs of digital broad-band seismograph stations in the Middle East. Twelve earthquakes selected in this way are plotted on the map in Figure 1. Differences between the directions of approach at each station and the great-circle path between stations range between 1.0 and 7.6 degrees, with most deviations being between about 2 and 6 degrees. Of the stations shown in Figure 1, 6 pairs (GNI-ABKT, ABKT-KIV, GNI-ANTO, ANTO-GNI, ANTO-KIV, and GNI-KIV) have, up to now, yielded useful data. Four of the earthquakes occurred beneath the Mediterranean Sea; for that reason, paths between the earthquakes cross oceanic-continental margins that may laterally refract the recorded surface waves at one or both stations, causing wave propagation directions to differ from the deviations given in Table 1. In addition, some paths, such as that between ANTO and KIV and between GNI and ABKT, cross regions known to be characterized by oceanic crust (in the former case the Black Sea and in the latter the southern Caspian Sea).

Examples showing the determination of phase and group velocities for Rayleigh and Love waves between stations GNI and ANTO appear in Figures 2-4. This is a path through eastern Turkey. Figures 2 and 3 show single-station determinations at the two stations and Figure 4 shows the interstation results. Similar determinations were done for all of the events in Figure 1 and Table 1.

Figure 5 presents 12 interstation determinations of Rayleigh wave phase and group velocity. Large variations, especially for group velocities at shorter periods, occur from path to path. At longer periods velocities are similar to those of the Basin and Range province in the western United States (Lin, 1989), another tectonically active region. At periods shorter than about 25 s the fastest group velocities are about 2.9 km/s, values that are again similar to those in the Basin and Range. Several velocities are, however, much lower (as small as 2.2 km/s) than the Basin and Range velocities of Lin (1989). The fastest

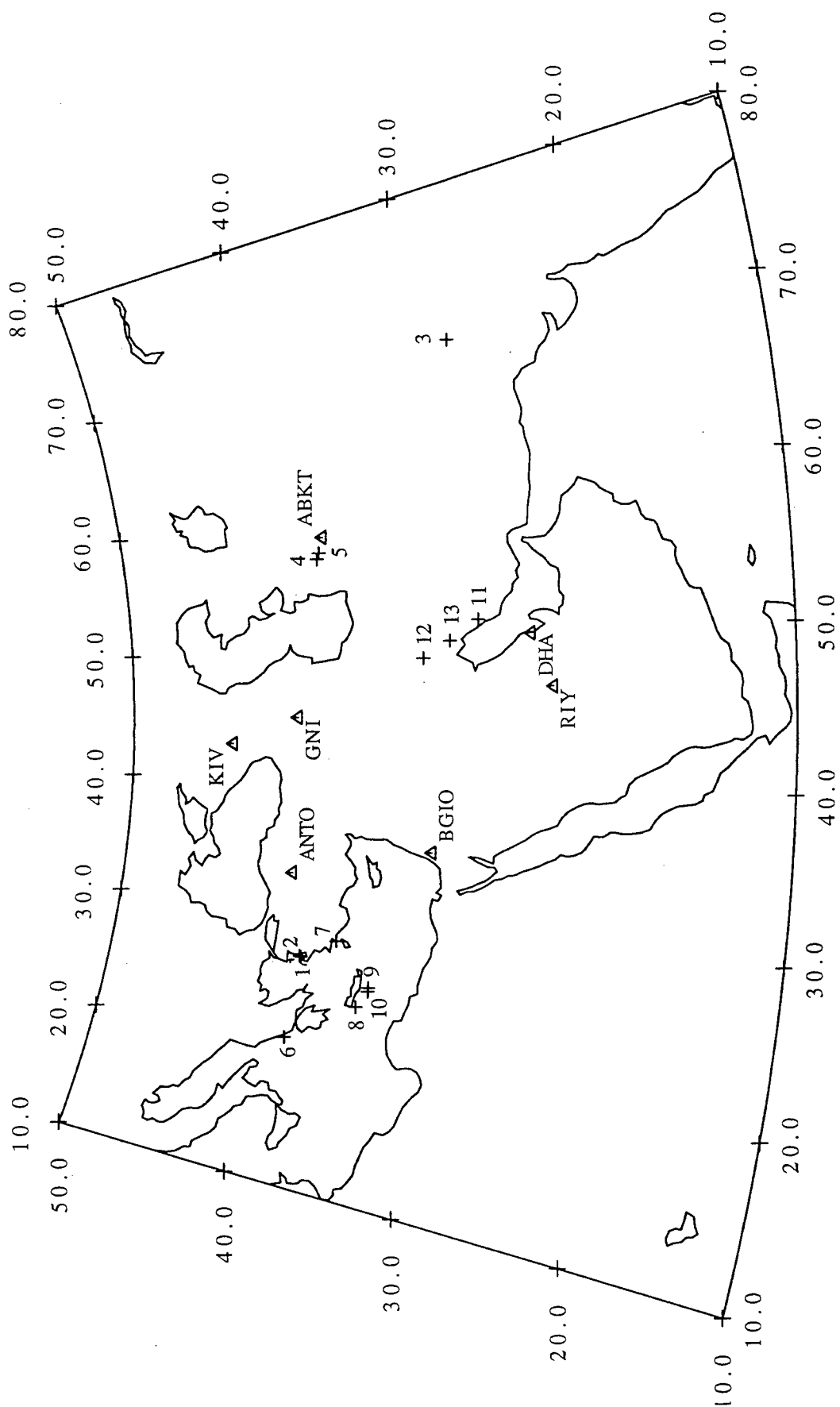


Figure 1

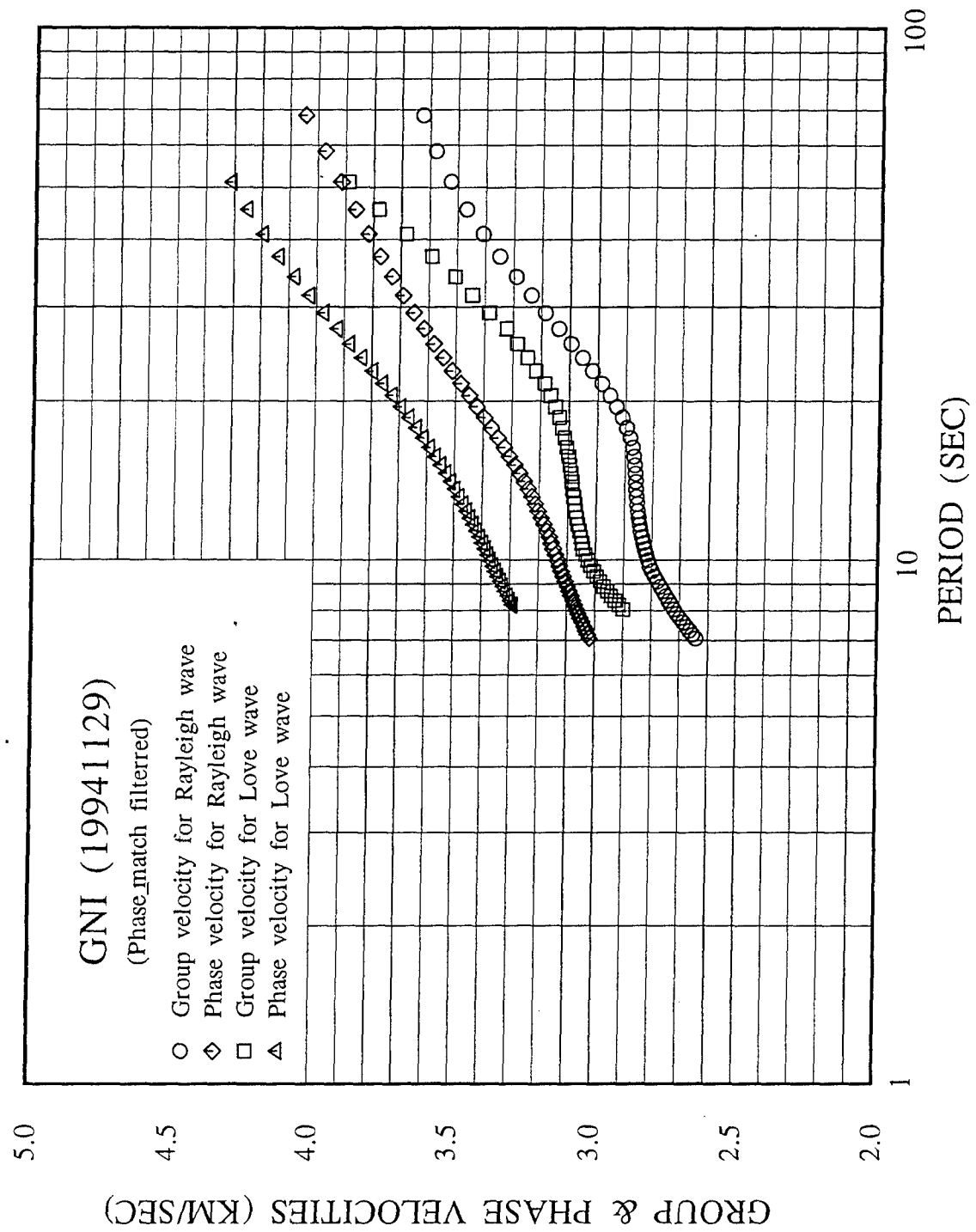


Figure 2

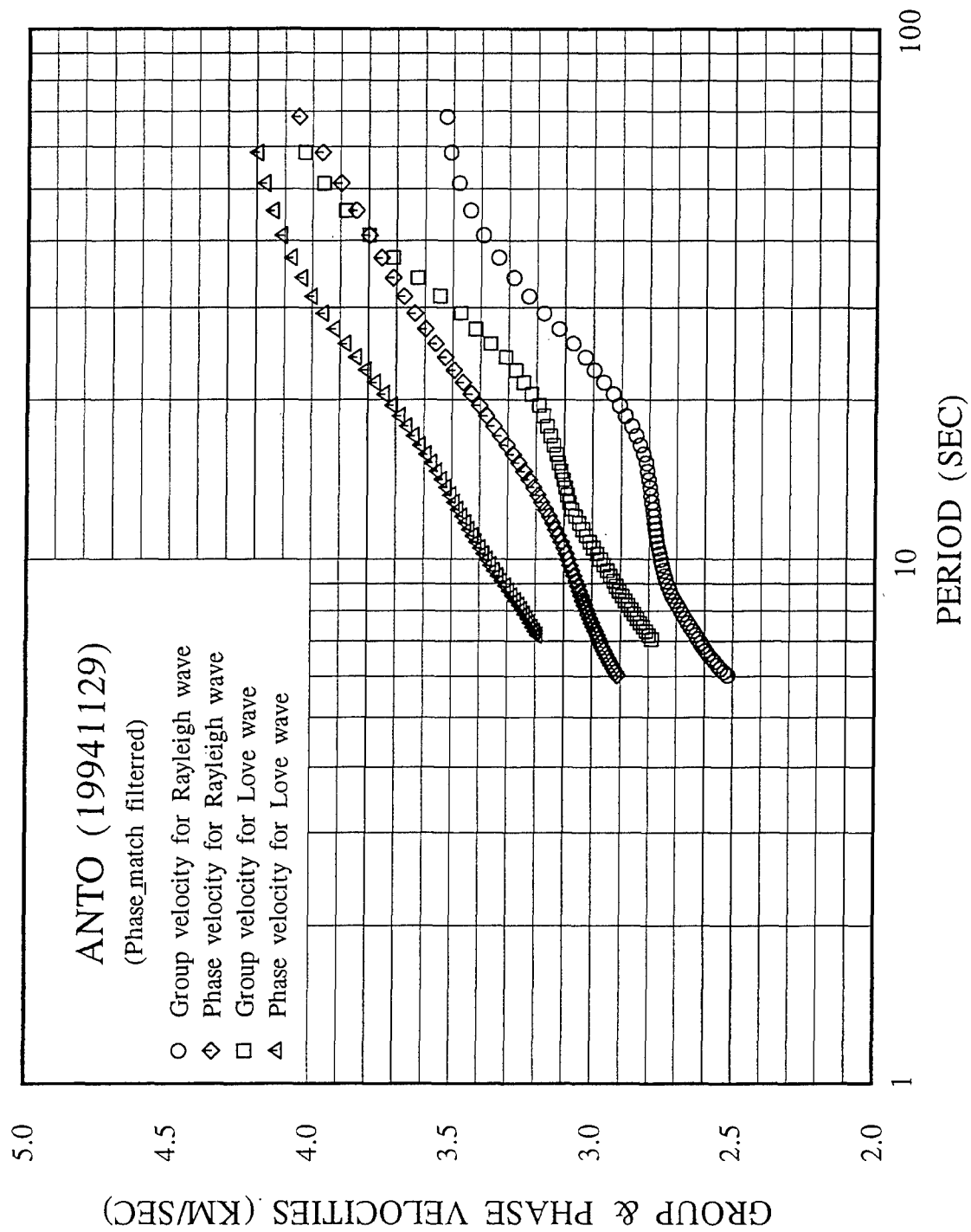


Figure 3

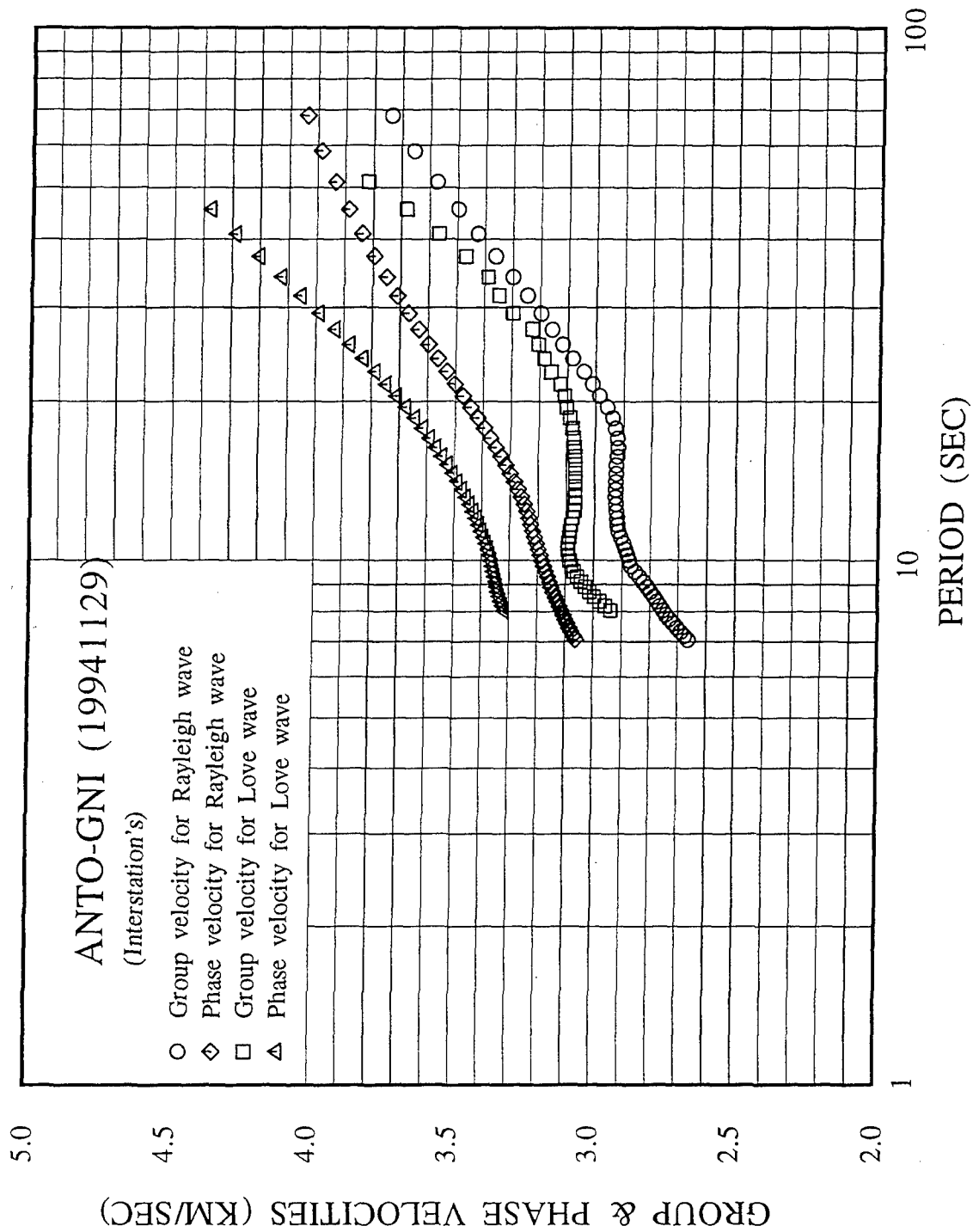


Figure 4

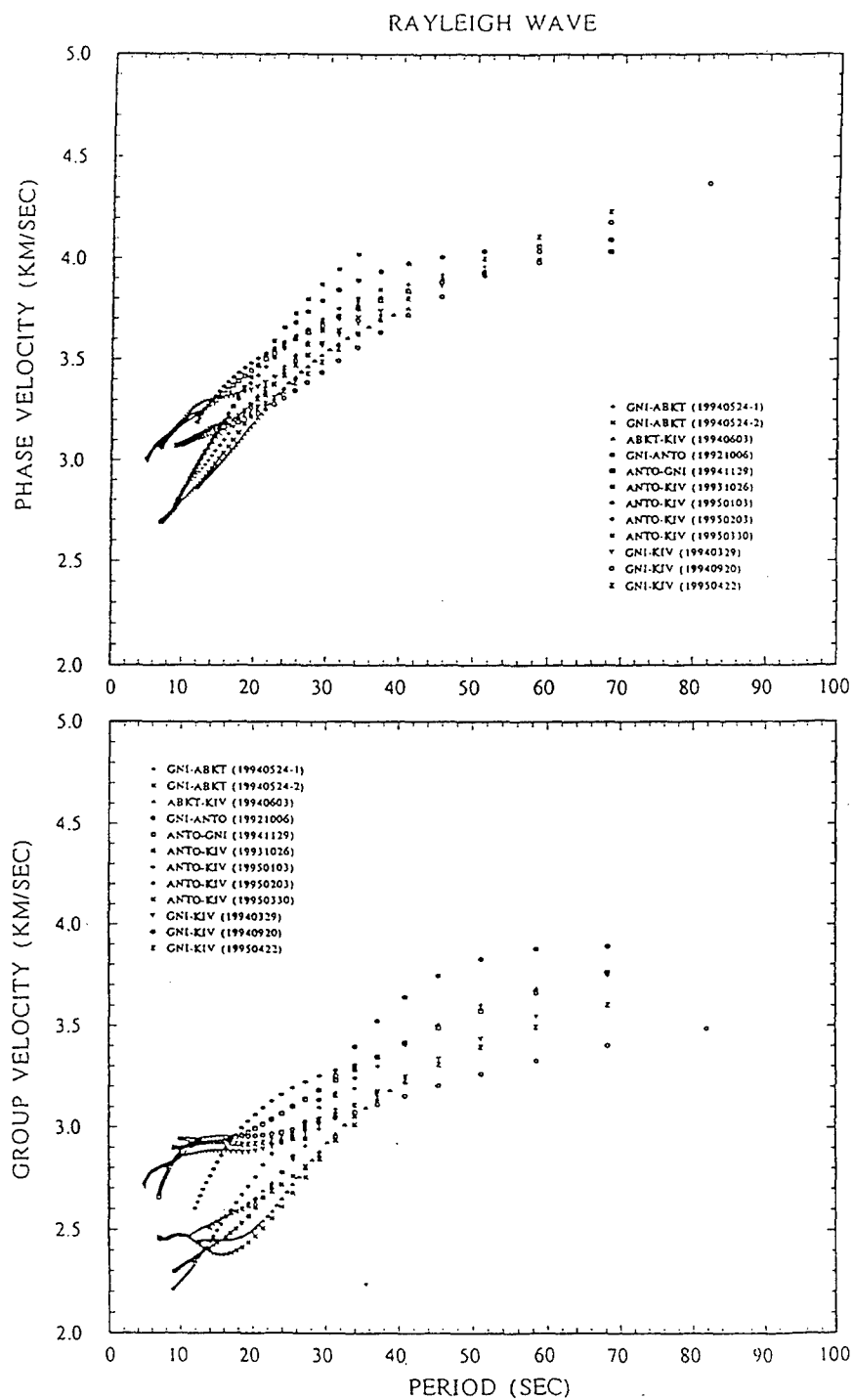


Figure 5

Table 1. Earthquakes for Two-station Method

Number	Date	Origin			Lat (° N)	Lon (° E)	Depth (km)	m_b	Stations	Az-dev 1 (°)	Az-dev 2 (°)
		h	m	s							
1	24 May 94	02	05	36.2	38.66	26.54	17	5.0	GNI-ABKT	7.1	4.1
2	24 May 94	02	18	34.9	38.76	26.60	16	5.0	GNI-ABKT	7.8	3.9
3	03 Jun 94	22	40	21.2	28.74	70.07	33	5.9	ABKT_KIV	6.9	3.6
4	06 Oct 92	08	57	17.7	38.42	56.52	10	4.7	GNI-ANTO	3.6	1.9
5	21 Oct 94	11	46	27.6	38.25	56.96	33	4.9	GNI-ANTO	4.1	2.2
6	29 Nov 94	14	30	28.4	38.71	20.48	21	4.9	ANTO-GNI	2.0	1.0
7	26 Oct 93	10	03	57.5	36.74	28.05	33	5.3	ANTO-KIV	6.3	2.3
8	03 Jan 95	22	51	45.0	34.94	23.55	33	4.9	ANTO-KIV	1.3	0.7
9	03 Feb 95	22	29	13.3	34.42	25.03	49	4.8	ANTO-KIV	6.7	3.3
10	30 Mar 95	18	17	15.1	34.40	24.79	7	4.9	ANTO-KIV	5.8	2.9
11	29 Mar 94	07	56	53.9	29.10	51.26	33	5.4	GNI-KIV	7.6	5.7
12	20 Sep 94	05	51	46.0	32.50	48.77	33	5.0	GNI-KIV	4.1	2.7
13	22 Apr 95	00	21	48.6	30.89	49.91	25	5.1	GNI-KIV	5.8	4.1

Rayleigh wave group velocities are those between stations GNI and KIV west of the Black Sea, suggesting that the crust is either thinner or faster than normal in that region.

We assume, after removing effects of wavefront spreading, that the spectral amplitudes (A) of seismic surface waves attenuate as $A(f) \sim e^{-\gamma(f)x}$ where f is frequency, γ is the attenuation coefficient in km^{-1} , and x is distance in km. The attenuation coefficients determined as a function of period appear in Figure 6. As with velocities, the attenuation coefficient values exhibit large variations from path-to-path. Mean values at periods of 30 s and greater are about $0.4 \times 10^{-3} \text{ km}^{-1}$. At shorter periods, they increase rapidly with decreasing periods reaching about $0.7 \times 10^{-3} \text{ km}^{-1}$ at 20 s and $1.7 \times 10^{-3} \text{ km}^{-1}$ at 10 s. These can be compared to the mean interstation values of Lin (1989) for the Basin and Range province, a region of crustal extension (with moderate tectonic activity), where seismic wave attenuation in the upper crust is known to be high (Lin, 1989; Mitchell and Xie, 1994). Attenuation coefficients in the Basin and Range are about $0.3 \times 10^{-3} \text{ km}^{-1}$ at periods greater than about 30 s, $0.35 \times 10^{-3} \text{ km}^{-1}$ at 20 s, and $0.66 \times 10^{-3} \text{ km}^{-1}$ at 10 s.

Attenuation coefficients obtained from interstation measurements in the Middle East are, therefore, higher at all periods than those determined for the Basin and Range using the same method. Mitchell (1995) has proposed that seismic Q (a quantity proportional to the inverse of attenuation) in any region is proportional to the length of time that has passed since the last episode of major tectonic activity there. For both the Middle East and Basin and Range to conform to that rule, they should both be characterized by the same attenuation since both are currently active. Since attenuation in the Middle East is higher than that in the Basin and Range, another factor, probably the greater intensity of deformation in the Middle East, must be responsible.

A New Tool for Surface Wave Dispersion and Polarization Analysis

The large variations of surface wave velocities and attenuation throughout the Middle East, that are apparent in Figures 5 and 6, suggest that our measured values could be significantly biased by deviations from assumed great-circle paths and by scattering due to lateral complexities in the crust and upper mantle. In addition, the wave forms of many of the surface waves that we found sometimes exhibit choppiness and other departures from the smooth character that we find in many other regions. Because of these complexities it will be important to determine the particle motion of the surface waves that we study. We have recently completed coding for a new program to determine surface wave dispersion and polarization as a function of period or frequency. The program SPAN (surface-wave polarization analysis), is a GUI program written for an X-window environment.

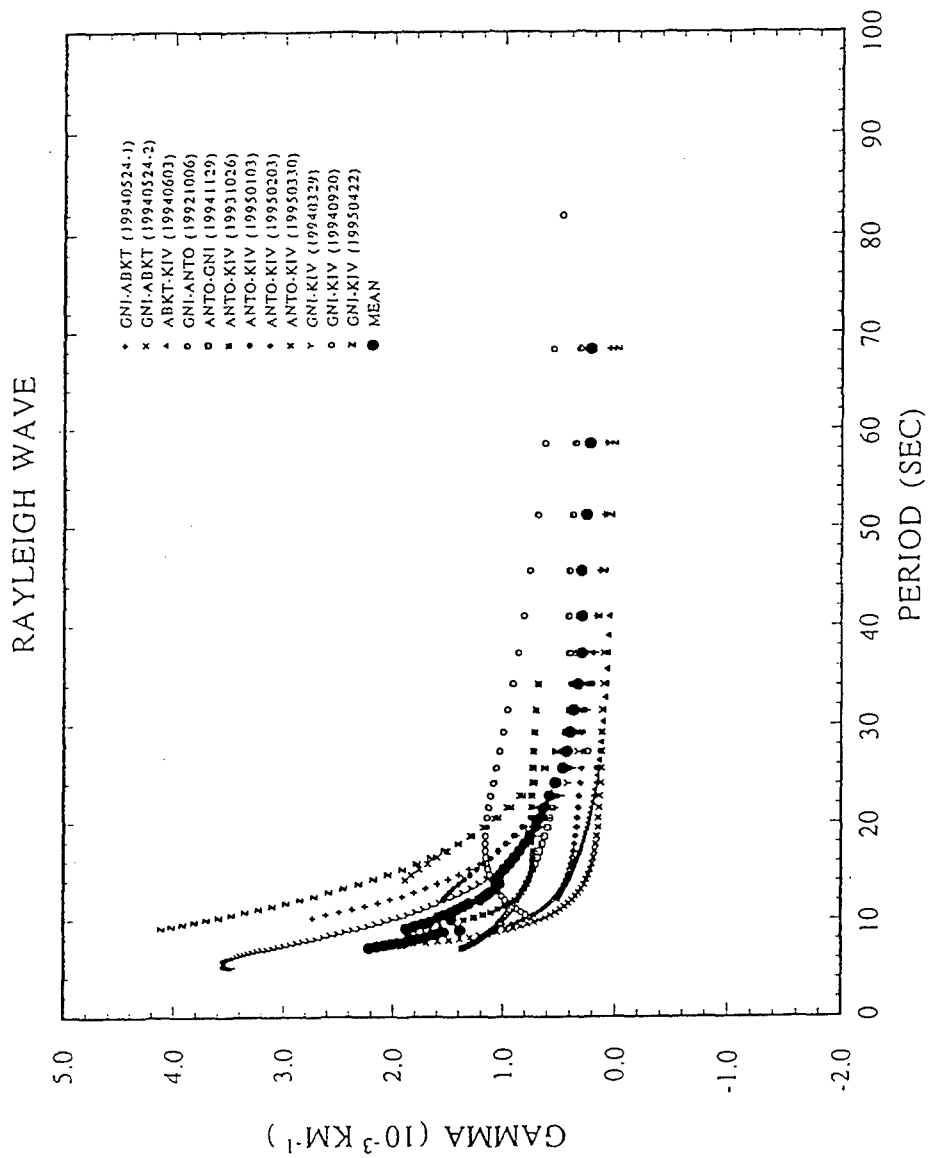


Figure 6

Dispersion can be determined using single-component records whereas polarization measurements require records of three components of motion. The computational procedures follow Levshin et al. (1992), but our implementation differs from that work by permitting researchers to proceed interactively through the process using results of each step to decide on parameters to be used in the next step. The procedure includes (1) plotting digital time series and displaying a dynamic plot of particle motion within any selected time window, (2) providing a view of the selected trace(s) in which one can select a time window of interest and apply selected window parameters (length of time window and slopes at the ends of the window) as shown in Figure 7, (3) determining the Fourier spectra for the selected portions of all traces, also shown in Figure 4, (4) displaying dispersion, obtained by means of the multiple-filter method, using color shading for various amplitude ranges (See Figure 8 for a gray-scale version), and (5) plotting deviations of particle motion polarization (including inclination, tilt, and slope of the polarization ellipse), again with color shading, from that expected for a plane-layered earth model (Figure 8). For Rayleigh waves ellipticity is also determined. In each step the user controls the process interactively using control panels in the active window.

Results are displayed for each step and can be saved and/or printed at the users discretion. Messages are displayed that prompt the user for the next step and manual instructions are accessible using help buttons. Dispersion curves are presented as contoured normalized amplitudes on a group velocity-period (or frequency) plot, where the amplitude maxima correspond to group velocities. Phase-equalization and time-variable filtration are used to isolate the desired mode for improved determinations of group or phase velocity.

Our future work will use SPAN to routinely determine particle motion in our surface wave analyses. Surface waves that are found to deviate greatly from a great circle path or exhibit particle motion that does not correspond to expected Rayleigh wave or Love wave motion, perhaps because of mode conversion, will not be used in our modeling of velocity or Q structure in the Middle East.

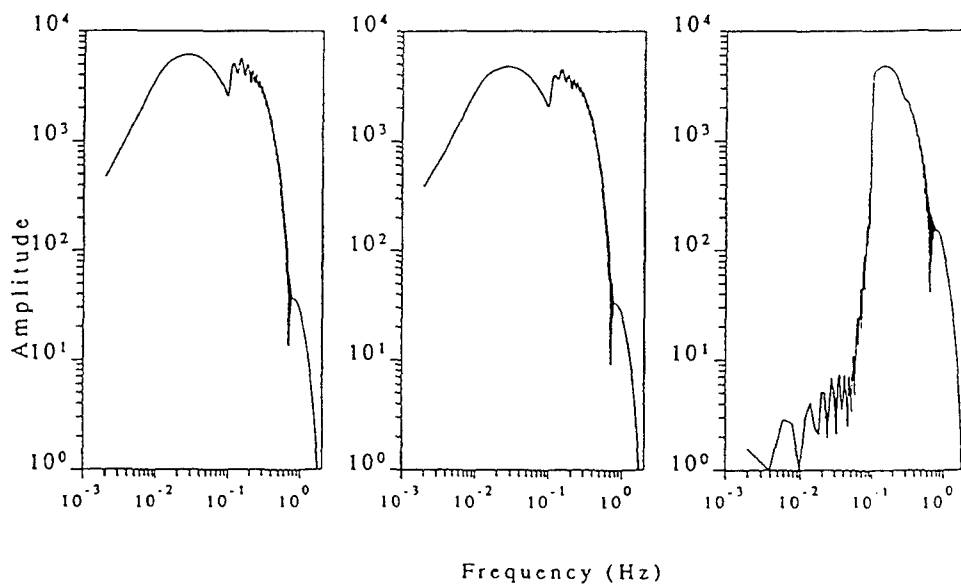
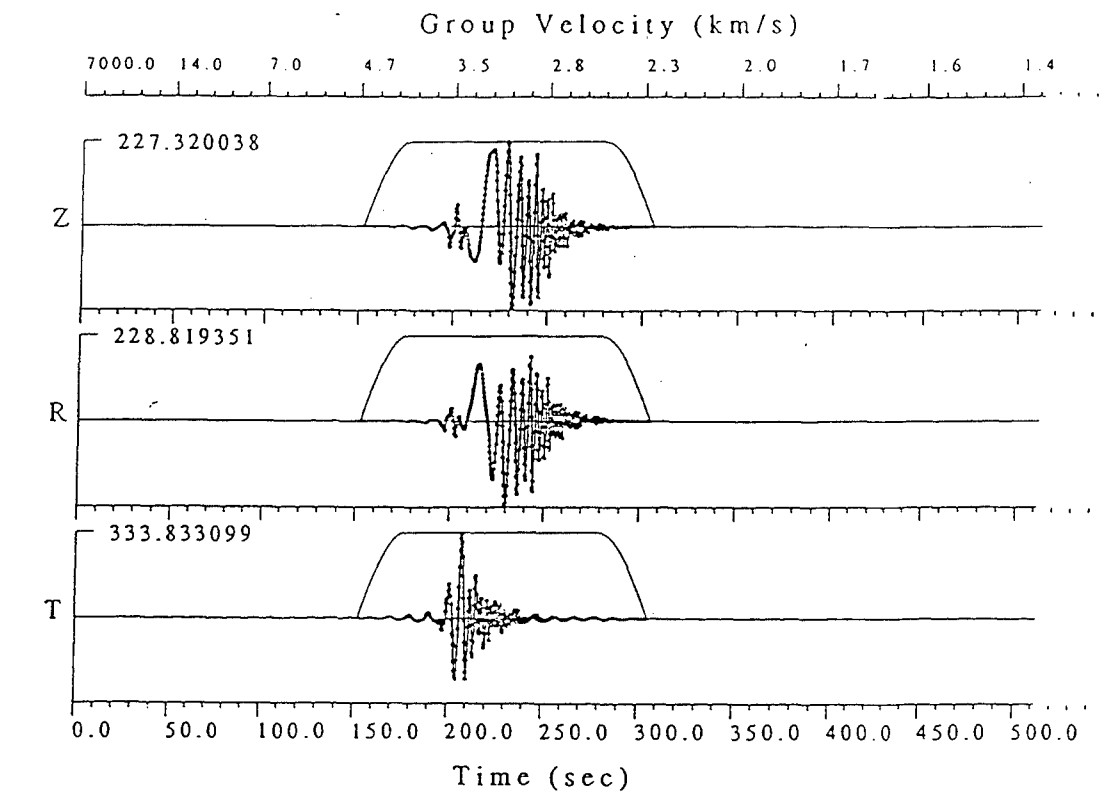


Figure 7

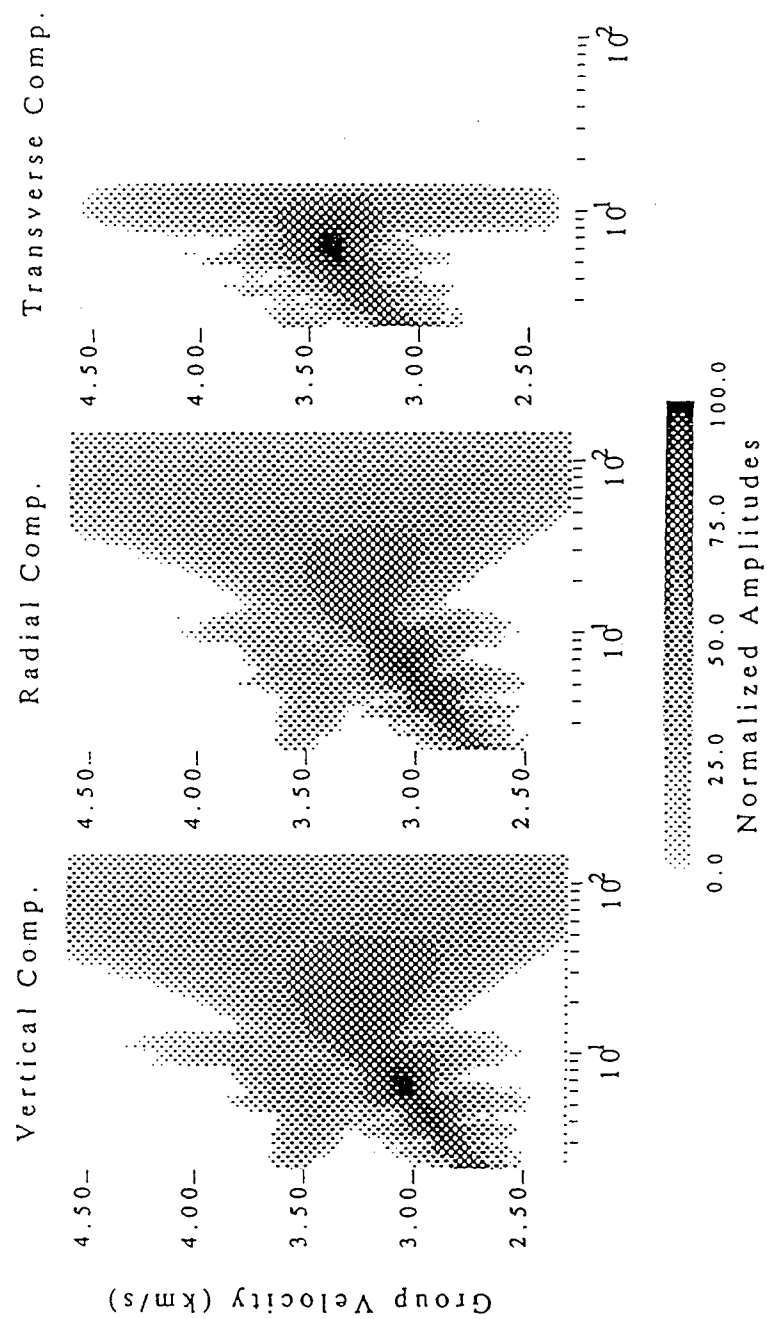


Figure 8

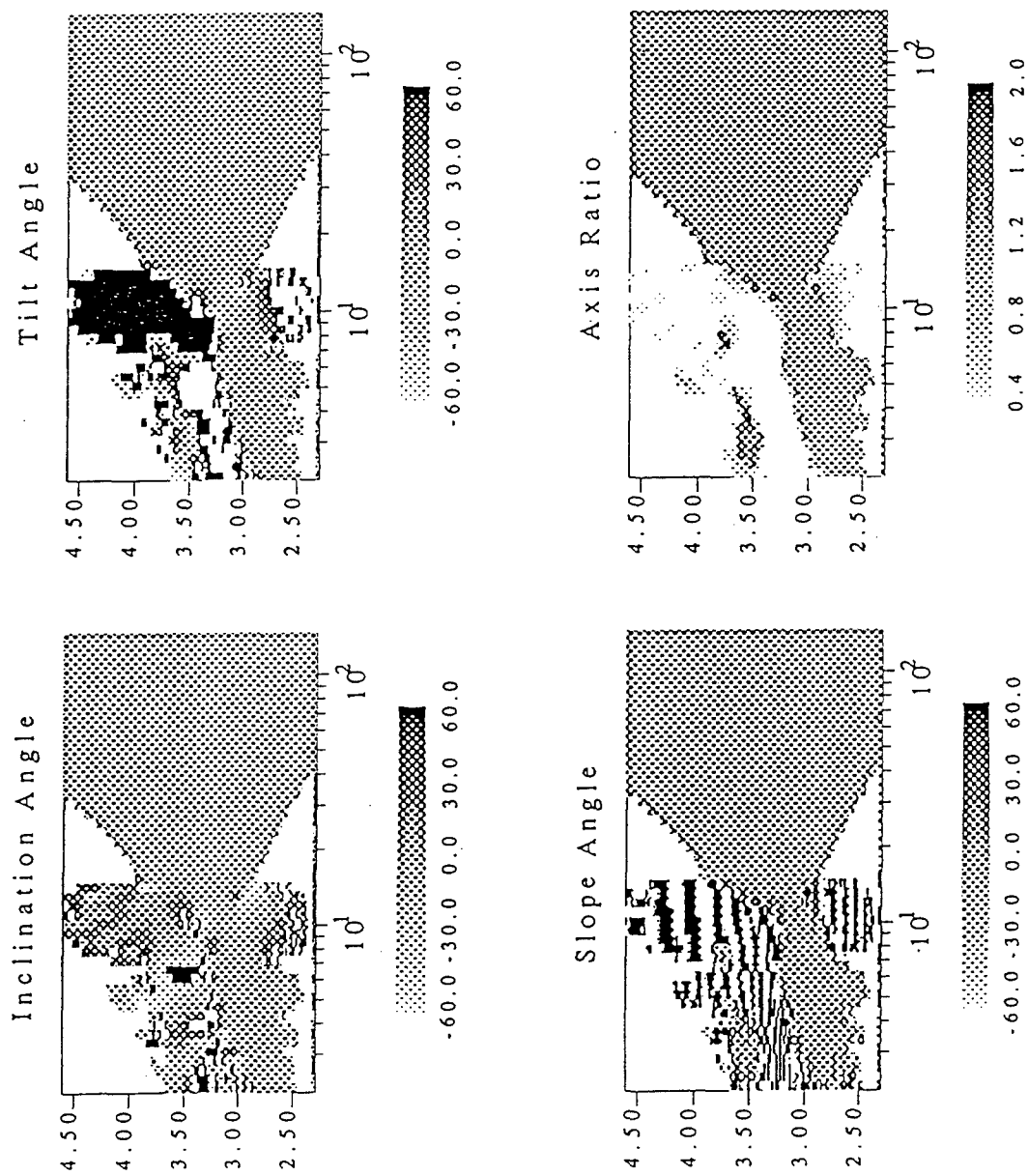


Figure 9

References

- Ghalib, H. Seismic velocity structure and attenuation of the Arabian plate, *Ph.D. dissertation*, 314 pp., Saint Louis University, St. Louis, MO, 1992.
- Levshin, A., L. Ratnikova, and J. Berger, Peculiarities of surface-wave propagation across central Eurasia, *Bull. Seism. Soc. Am.*, 82, 2464-2493, 1992.
- Lin, W.J., Rayleigh attenuation in the Basin and Range province, *M.S. thesis*, 55 pp. Saint Louis University, St. Louis, MO, 1989.
- Mitchell, B.J., Anelastic structure and evolution of the continental crust and upper mantle from seismic surface wave attenuation, *Rev. Geophys.*, 33, 441-462, 1995.
- Mitchell, B.J., Y. Pan, and J. Xie, The variation of Lg coda Q across Eurasia and its relation to continental evolution, *J. Geophys. Res.*, submitted, 1996.
- Molnar, P., and Tapponnier, Cenozoic tectonics of Asia: Effects of a continental collision, *Science*, 189, 419-426, 1975.
- Nuttli, O.W., The excitation and attenuation of seismic crustal phases in Iran, *Bull. Seism. Soc. Am.*, 70, 469-485, 1980.
- Seber, D., and B.J. Mitchell, Attenuation of surface waves across the Arabian peninsula, *Tectonophysics*, 204, 137-150, 1992.
- Sengör, A.M.C., Tectonics of the Tethysides: Orogenic collage development in a collisional setting, in *Ann. Rev. Earth Planet. Sci.*, 15, 213-244, 1987.

THOMAS AHRENS
SEISMOLOGICAL LABORATORY 252-21
CALIFORNIA INSTITUTE OF TECHNOLOGY
PASADENA, CA 91125

RALPH ALEWINE
NTPO
1901 N. MOORE STREET, SUITE 609
ARLINGTON, VA 22209

* LOS ALAMOS NATIONAL LABORATORY
ATTN: TECHNICAL STAFF (PLS ROUTE)
PO BOX 1663,
* MS F659
LOS ALAMOS, NM 87545

LAWRENCE LIVERMORE NATIONAL LABORATORY
ATTN: TECHNICAL STAFF (PLS ROUTE)
PO BOX 808,
MS L-200
LIVERMORE, CA 94551

MUAWIA BARAZANGI
INSTITUTE FOR THE STUDY OF THE CONTINENTS
3126 SNEE HALL
CORNELL UNIVERSITY
ITHACA, NY 14853

RICHARD BARDZELL
ACIS
DCI/ACIS
WASHINGTON, DC 20505

T.G. BARKER
MAXWELL TECHNOLOGIES
P.O. BOX 23558
SAN DIEGO, CA 92123

DOUGLAS BAUMGARDT
ENSCO INC.
5400 PORT ROYAL ROAD
SPRINGFIELD, VA 22151

SANDIA NATIONAL LABORATORY
ATTN: TECHNICAL STAFF (PLS ROUTE)
DEPT. 5791
MS 0567, PO BOX 5800
ALBUQUERQUE, NM 87185-0567

THERON J. BENNETT
MAXWELL TECHNOLOGIES
11800 SUNRISE VALLEY DRIVE SUITE 1212
RESTON, VA 22091

WILLIAM BENSON
NAS/COS
ROOM HA372
2001 WISCONSIN AVE. NW
WASHINGTON, DC 20007

JONATHAN BERGER
UNIVERSITY OF CA, SAN DIEGO
SCRIPPS INSTITUTION OF OCEANOGRAPHY IGPP, 0225
9500 GILMAN DRIVE
LA JOLLA, CA 92093-0225

ROBERT BLANDFORD
AFTAC
1300 N. 17TH STREET
SUITE 1450
ARLINGTON, VA 22209-2308

LOS ALAMOS NATIONAL LABORATORY
ATTN: TECHNICAL STAFF (PLS ROUTE)
PO BOX 1663, MS F665
LOS ALAMOS, NM 87545

LAWRENCE LIVERMORE NATIONAL LABORATORY
ATTN: TECHNICAL STAFF (PLS ROUTE)
PO BOX 808, MS L-207
LIVERMORE, CA 94551

STEVEN BRATT
NTPO
1901 N. MOORE STREET, SUITE 609
ARLINGTON, VA 22209

SANDIA NATIONAL LABORATORY
ATTN: TECHNICAL STAFF (PLS ROUTE)
DEPT. 5704
MS 0655, PO BOX 5800
* ALBUQUERQUE, NM 87185-0655

LAWRENCE LIVERMORE NATIONAL LABORATORY
ATTN: TECHNICAL STAFF (PLS ROUTE)
PO BOX 808, MS L-221
LIVERMORE, CA 94551

RHETT BUTLER
IRIS
1616 N. FORT MEYER DRIVE
SUITE 1050
ARLINGTON, VA 22209

SANDIA NATIONAL LABORATORY
ATTN: TECHNICAL STAFF (PLS ROUTE)
DEPT. 5736
MS 0655, PO BOX 5800
ALBUQUERQUE, NM 87185-0655

LESLIE A. CASEY
DOE
1000 INDEPENDENCE AVE. SW
NN-40
WASHINGTON, DC 20585-0420

DR. STANLEY DICKINSON
AFOSR
110 DUNCAN AVENUE
SUITE B115
BOLLING AFB, WASHINGTON D.C. 20332-001

DIANE I. DOSER
DEPARTMENT OF GEOLOGICAL SCIENCES
THE UNIVERSITY OF TEXAS AT EL PASO
EL PASO, TX 79968

SANDIA NATIONAL LABORATORY
ATTN: TECHNICAL STAFF (PLS ROUTE)
SNL, DEPT. 4115
MS 0329, PO BOX 5800
ALBUQUERQUE, NM 87185-0329

JOHN FILSON
ACIS/TMG/NTT
ROOM 6T11 NHB
WASHINGTON, DC 20505

LAWRENCE LIVERMORE NATIONAL LABORATORY
ATTN: TECHNICAL STAFF (PLS ROUTE)
PO BOX 808, MS L-208
LIVERMORE, CA 94551

ROBERT GEIL
DOE
PALAIS DES NATIONS, RM D615
GENEVA 10, SWITZERLAND

HENRY GRAY
SMU STATISTICS DEPARTMENT
P.O. BOX 750302
DALLAS, TX 75275-0302

PACIFIC NORTHWEST NATIONAL LABORATORY
ATTN: TECHNICAL STAFF (PLS ROUTE)
PO BOX 999, MS K7-34
RICHLAND, WA 99352

JAMES HAYES
NSF
4201 WILSON BLVD., ROOM 785
ARLINGTON, VA 22230

SANDIA NATIONAL LABORATORY
ATTN: TECHNICAL STAFF (PLS ROUTE)
DEPT. 9311
MS 1159, PO BOX 5800
ALBUQUERQUE, NM 87185-1159

SEAN DORAN
ACIS
DCI/ACIS
WASHINGTON, DC 20505

LAWRENCE LIVERMORE NATIONAL LABORATORY
ATTN: TECHNICAL STAFF (PLS ROUTE)
LLNL
PO BOX 808, MS L-175
LIVERMORE, CA 94551

RICHARD J. FANTEL
BUREAU OF MINES
DEPT OF INTERIOR, BLDG 20
DENVER FEDERAL CENTER
DENVER, CO 80225

MARK D. FISK
MISSION RESEARCH CORPORATION
735 STATE STREET
P.O. DRAWER 719
SANTA BARBARA, CA 93102-0719

PACIFIC NORTHWEST NATIONAL LABORATORY
ATTN: TECHNICAL STAFF (PLS ROUTE)
PO BOX 999, MS K6-48
RICHLAND, WA 99352

LORI GRANT
MULTIMAX, INC.
311C FOREST AVE. SUITE 3
PACIFIC GROVE, CA 93950

CATHERINE DE GROOT-HEDLIN
SCRIPPS INSTITUTION OF OCEANOGRAPHY
UNIVERSITY OF CALIFORNIA, SAN DIEGO
INSTITUTE OF GEOPHYSICS AND PLANETARY PHYSICS
LA JOLLA, CA 92093

PACIFIC NORTHWEST NATIONAL LABORATORY
ATTN: TECHNICAL STAFF (PLS ROUTE)
PO BOX 999, MS K6-40
RICHLAND, WA 99352

THOMAS HEARN
NEW MEXICO STATE UNIVERSITY
DEPARTMENT OF PHYSICS
LAS CRUCES, NM 88003

MICHAEL HEDLIN
UNIVERSITY OF CALIFORNIA, SAN DIEGO
SCRIPPS INSTITUTION OF OCEANOGRAPHY IGPP, 0225
9500 GILMAN DRIVE
LA JOLLA, CA 92093-0225

• EUGENE HERRIN
SOUTHERN METHODIST UNIVERSITY
DEPARTMENT OF GEOLOGICAL SCIENCES
• DALLAS, TX 75275-0395

VINDELL HSU
HQ/AFTAC/TTR
1030 S. HIGHWAY A1A
PATRICK AFB, FL 32925-3002

THOMAS JORDAN
MASSACHUSETTS INSTITUTE OF TECHNOLOGY
EARTH, ATMOSPHERIC & PLANETARY SCIENCES
77 MASSACHUSETTS AVENUE, 54-918
CAMBRIDGE, MA 02139

ANATOLI L. LEVSHIN
DEPARTMENT OF PHYSICS
UNIVERSITY OF COLORADO
CAMPUS BOX 390
BOULDER, CO 80309-0309

GARY MCCARTOR
SOUTHERN METHODIST UNIVERSITY
DEPARTMENT OF PHYSICS
DALLAS, TX 75275-0395

PACIFIC NORTHWEST NATIONAL LABORATORY
ATTN: TECHNICAL STAFF (PLS ROUTE)
PO BOX 999, MS K7-22
RICHLAND, WA 99352

RICHARD MORROW
USACDA/IVI
320 21ST STREET, N.W.
WASHINGTON, DC 20451

JAMES NI
• NEW MEXICO STATE UNIVERSITY
DEPARTMENT OF PHYSICS
• LAS CRUCES, NM 88003

JOHN ORCUTT
INSTITUTE OF GEOPHYSICS AND PLANETARY PHYSICS
UNIVERSITY OF CALIFORNIA, SAN DIEGO
LA JOLLA, CA 92093

DONALD HELMBERGER
CALIFORNIA INSTITUTE OF TECHNOLOGY
DIVISION OF GEOLOGICAL & PLANETARY SCIENCES
SEISMOLOGICAL LABORATORY
PASADENA, CA 91125

ROBERT HERRMANN
ST. LOUIS UNIVERSITY
DEPARTMENT OF EARTH & ATMOSPHERIC SCIENCES
3507 LACLEDE AVENUE
ST. LOUIS, MO 63103

ANTHONY IANNACCHIONE
BUREAU OF MINES
COCHRANE MILL ROAD
PO BOX 18070
PITTSBURGH, PA 15236-9986

THORNE LAY
UNIVERSITY OF CALIFORNIA, SANTA CRUZ
EARTH SCIENCES DEPARTMENT
EARTH & MARINE SCIENCE BUILDING
SANTA CRUZ, CA 95064

DONALD A. LINGER
DNA
6801 TELEGRAPH ROAD
ALEXANDRIA, VA 22310

KEITH MCLAUGHLIN
MAXWELL TECHNOLOGIES
P.O. BOX 23558
SAN DIEGO, CA 92123

BRIAN MITCHELL
DEPARTMENT OF EARTH & ATMOSPHERIC SCIENCES
ST. LOUIS UNIVERSITY
3507 LACLEDE AVENUE
ST. LOUIS, MO 63103

JOHN MURPHY
MAXWELL TECHNOLOGIES
11800 SUNRISE VALLEY DRIVE SUITE 1212
RESTON, VA 22091

CHARLES ODDENINO
BUREAU OF MINES
810 7TH ST. NW
WASHINGTON, DC 20241

FRANK PILOTTE
HQ/AFTAC/TT
1030 S. HIGHWAY A1A
PATRICK AFB, FL 32925-3002

KEITH PRIESTLEY
DEPARTMENT OF EARTH SCIENCES
UNIVERSITY OF CAMBRIDGE
MADINGLEY RISE, MADINGLEY ROAD
CAMBRIDGE, CB3 0EZ UK

PACIFIC NORTHWEST NATIONAL LABORATORY
ATTN: TECHNICAL STAFF (PLS ROUTE)
PO BOX 999, MS K5-72
RICHLAND, WA 99352

PACIFIC NORTHWEST NATIONAL LABORATORY
ATTN: TECHNICAL STAFF (PLS ROUTE)
PO BOX 999, MS K6-84
RICHLAND, WA 99352

CHANDAN SAIKIA
WOODWARD-CLYDE FEDERAL SERVICES
566 EL DORADO ST., SUITE 100
PASADENA, CA 91101-2560

AVI SHAPIRA
SEISMOLOGY DIVISION
THE INSTITUTE FOR PETROLEUM RESEARCH AND
GEOPHYSICS
P.O.B. 2286, NOLON 58122 ISRAEL

MATTHEW SIBOL
ENSCO, INC.
445 PINEDA COURT
MELBOURNE, FL 32940

LOS ALAMOS NATIONAL LABORATORY
ATTN: TECHNICAL STAFF (PLS ROUTE)
PO BOX 1663, MS D460
LOS ALAMOS, NM 87545

LAWRENCE LIVERMORE NATIONAL LABORATORY
ATTN: TECHNICAL STAFF (PLS ROUTE)
PO BOX 808, MS L-195
LIVERMORE, CA 94551

LOS ALAMOS NATIONAL LABORATORY
ATTN: TECHNICAL STAFF (PLS ROUTE)
PO BOX 1663, MS C335
LOS ALAMOS, NM 87545

DAVID THOMAS
ISEE
29100 AURORA ROAD
CLEVELAND, OH 44139

JAY PULLI
RADIX SYSTEMS, INC.
6 TAFT COURT
ROCKVILLE, MD 20850

PAUL RICHARDS
COLUMBIA UNIVERSITY
LAMONT-DOHERTY EARTH OBSERVATORY
PALISADES, NY 10964

LAWRENCE LIVERMORE NATIONAL LABORATORY
ATTN: TECHNICAL STAFF (PLS ROUTE)
PO BOX 808, MS L-202
LIVERMORE, CA 94551

THOMAS SERENO JR.
SCIENCE APPLICATIONS INTERNATIONAL
CORPORATION
10260 CAMPUS POINT DRIVE
SAN DIEGO, CA 92121

ROBERT SHUMWAY
410 MRAK HALL
DIVISION OF STATISTICS
UNIVERSITY OF CALIFORNIA
DAVIS, CA 95616-8671

SANDIA NATIONAL LABORATORY
ATTN: TECHNICAL STAFF (PLS ROUTE)
DEPT. 5704
MS 0979, PO BOX 5800
ALBUQUERQUE, NM 87185-0979

DAVID SIMPSON
IRIS
1616 N. FORT MEYER DRIVE
SUITE 1050
ARLINGTON, VA 22209

JEFFRY STEVENS
MAXWELL TECHNOLOGIES
P.O. BOX 23558
SAN DIEGO, CA 92123

BRIAN SULLIVAN
BOSTON COLLEGE
INSITUTE FOR SPACE RESEARCH
140 COMMONWEALTH AVENUE
CHESTNUT HILL, MA 02167

NAFI TOKSOZ
EARTH RESOURCES LABORATORY, M.I.T.
42 CARLTON STREET, E34-440
CAMBRIDGE, MA 02142

LAWRENCE TURNBULL
ACIS
DCI/ACIS
WASHINGTON, DC 20505

* GREG VAN DER VINK
IRIS
1616 N. FORT MEYER DRIVE
* SUITE 1050
ARLINGTON, VA 22209

LAWRENCE LIVERMORE NATIONAL LABORATORY
ATTN: TECHNICAL STAFF (PLS ROUTE)
PO BOX 808, MS L-205
LIVERMORE, CA 94551

JAMES WHITCOMB
NSF
NSF/ISC OPERATIONS/EAR-785
4201 WILSON BLVD., ROOM 785
ARLINGTON, VA 22230

JIANG XIE
COLUMBIA UNIVERSITY
LAMONT DOHERTY EARTH OBSERVATORY
ROUTE 9W
PALISADES, NY 10964

SANDIA NATIONAL LABORATORY
ATTN: TECHNICAL STAFF (PLS ROUTE)
DEPT. 6116
MS 0750, PO BOX 5800
ALBUQUERQUE, NM 87185-0750

SECRETARY OF THE AIR FORCE
(SAFRD)
WASHINGTON, DC 20330

DEFENSE TECHNICAL INFORMATION CENTER
8725 JOHN J. KINGMAN ROAD
FT BELVOIR, VA 22060-6218 (2 COPIES)

* PHILLIPS LABORATORY
ATTN: XPG
29 RANDOLPH ROAD
* HANSCOM AFB, MA 01731-3010

PHILLIPS LABORATORY
ATTN: TSML
5 WRIGHT STREET
HANSCOM AFB, MA 01731-3004

FRANK VERNON
UNIVERSITY OF CALIFORNIA, SAN DIEGO
SCRIPPS INSTITUTION OF OCEANOGRAPHY IGPP, 0225
9500 GILMAN DRIVE
LA JOLLA, CA 92093-0225

TERRY WALLACE
UNIVERSITY OF ARIZONA
DEPARTMENT OF GEOSCIENCES
BUILDING #77
TUCSON, AZ 85721

DANIEL WEILL
NSF
EAR-785
4201 WILSON BLVD., ROOM 785
ARLINGTON, VA 22230

RU SHAN WU
UNIVERSITY OF CALIFORNIA SANTA CRUZ
EARTH SCIENCES DEPT.
1156 HIGH STREET
SANTA CRUZ, CA 95064

PACIFIC NORTHWEST NATIONAL LABORATORY
ATTN: TECHNICAL STAFF (PLS ROUTE)
PO BOX 999, MS K5-12
RICHLAND, WA 99352

JAMES E. ZOLLWEG
BOISE STATE UNIVERSITY
GEOSCIENCES DEPT.
1910 UNIVERSITY DRIVE
BOISE, ID 83725

OFFICE OF THE SECRETARY OF DEFENSE
DDR&E
WASHINGTON, DC 20330

TACTEC
BATTELLE MEMORIAL INSTITUTE
505 KING AVENUE
COLUMBUS, OH 43201 (FINAL REPORT)

PHILLIPS LABORATORY
ATTN: GPE
29 RANDOLPH ROAD
HANSCOM AFB, MA 01731-3010

PHILLIPS LABORATORY
ATTN: PL/SUL
3550 ABERDEEN AVE SE
KIRTLAND, NM 87117-5776 (2 COPIES)